Cholinergic neuron circadian clock mediates RNA-binding protein function and contributes to ALS disease phenotypes

Sharon B. Tam[1], Nathan J. Waldeck[2], Matthew Wright[1,3], Erin M. Baker[1], Evangelos Kiskinis[1,3], Joseph Bass[2], Robert G. Kalb[1*]

[1]The Ken & Ruth Davee Department of Neurology, Northwestern University Feinberg School of Medicine, Chicago, IL 60611, USA.
[2]Department of Medicine, Division of Endocrinology, Metabolism, and Molecular Medicine, Northwestern University Feinberg School of Medicine, Chicago, IL 60611, USA.
[3]Department of Neuroscience, Northwestern University Feinberg School of Medicine, Chicago, IL 60611, USA.

*Correspondence: robert.kalb1@northwestern.edu

Keywords: circadian clock, amyotrophic lateral sclerosis (ALS), RNA-binding protein (RBP), alternative splicing, transcriptomics, synaptic transmission, axonal transport

ABSTRACT

Circadian clocks are encoded by a transcription-translation feedback loop that aligns physiological processes with the solar cycle. Previous work linking the circadian clock to the regulation of RNA-binding proteins (RBPs) and alternative splicing provides a foundation for the vital examination of their mechanistic connections in the context of amyotrophic lateral sclerosis (ALS)—a fatal neurodegenerative disease characterized by disrupted RBP function. Here, we reveal enrichment of genes associated with ALS and other neurodegenerative diseases in the spinal cord cholinergic neuron rhythmic transcriptome. We demonstrate that there is circadian regulation of ALS-linked RBPs and rhythmic alternative splicing of genes involved in intracellular transport (*Aftph* and *Mvb12a*), microtubule cytoskeleton organization (*Limch1* and *Drc3*), and synaptic function (*Sipa1l2*) in this neuronal sub-type. Further, we show that the cholinergic neuron clock regulates sporadic ALS-associated changes in cytoskeleton and neuromuscular junction synapse gene expression. Finally, we report that cell-type-specific *Bmal1*-deletion *(i)* increases sciatic nerve axon degeneration, *(ii)* drives alternative splicing of genes encoding ALS-linked RBPs (*Matr3* and *Srsf7*), and *(iii)* drives alternative splicing of genes associated with microtubule transport and postsynaptic organization. Our results establish a role for the cholinergic neuron clock in RBP function and ALS disease phenotypes.

INTRODUCTION

The circadian system acts as a biological timekeeper that aligns physiological energetic cycles with the day/night cycle. In mammals, the molecular clock is encoded by a transcription-translation feedback loop comprised of activators (CLOCK and BMAL1) that induce the transcription of repressors (PERs and CRYs), which feedback to inhibit the forward limb in a cycle that repeats itself every ~24 hours, with a stabilizing loop consisting of REV-ERB and ROR transcription factors that modulate BMAL1 expression (Bass, 2012). In recent decades, clock transcriptional regulation has been characterized in diverse mammalian tissues and is estimated to drive the rhythmic expression of 10-15% of all mRNAs within a given tissue (Lowrey and Takahashi, 2004; Panda et al., 2002; Vollmers et al., 2009). Intriguingly, recent studies in liver have demonstrated that most of the genes that exhibit rhythmic mRNA expression do not exhibit rhythmic expression of the corresponding intron-containing pre-mRNA, suggesting that post-transcriptional modifications play a major role in the regulation of circadian gene expression (Green, 2018; Koike et al., 2012; Kojima et al., 2011; Menet et al., 2012).

Emerging evidence points to a connection between the circadian clock and RNA-processing events, such as methylation, polyadenylation, and alternative splicing (Fustin et al., 2013; Kojima et al., 2012; Marcheva et al., 2020). Time-of-day-dependent production of alternatively spliced transcripts has been previously reported in plants, flies, and mice, primarily in neuronal cell-types (Hughes et al., 2012; Marcheva et al., 2020; McGlincy et al., 2012; Sanchez et al., 2010; Wang et al., 2018; Yang et al., 2020). Alternative splicing allows a single gene to produce multiple distinct mRNA transcripts in a tissue- and cell-type specific manner, which contributes to transcriptomic diversity and enables cells to perform complex and specialized functions (Chen and Manley, 2009; Young et al., 1981). This process is strongly regulated by RNA-binding proteins (RBPs), which bind to specific regulatory sequence motifs in pre-mRNA and either enhance or suppress spliceosome recruitment to the splice sites (Ule and Blencowe, 2019). While RBPs are ubiquitously expressed, cells and tissue within the central nervous system (CNS) demonstrate greater disease vulnerability to RBP dysregulation due to their higher frequency of alternative splicing and more intricate transcriptomes (Pan et al., 2008; Yeo et al., 2004).

Disrupted RBP homeostasis is a hallmark of many neurological diseases, including amyotrophic lateral sclerosis (ALS), which is a progressive neurodegenerative disease that originates in upper and lower motor neurons in the brain and spinal cord (Nussbacher et al.,

2019; Prashad and Gopal, 2021). Genetic studies have revealed associations between ALS and mutations in genes encoding a number of RBPs, including TDP-43, FUS, ATXN2, TAF15, EWSR1, hnRNPA1, hnRNPA2B1, MATR3, and TIA1 (Kapeli et al., 2017; Zhao et al., 2018). These RBPs are key regulators of RNA metabolism and neuronal health, and ALS-linked mutations have been shown to vastly disrupt RNA processes, such as alternative splicing, mRNA transport, liquid phase transitions, and local translation (Kapeli et al., 2017; Nagano and Araki, 2021). For example, many of the proteins that co-purify with TDP-43 are associated with RNA splicing and translation (Freibaum et al., 2010), and ALS-linked mutations in TDP-43 were shown to impair mRNA axonal transport and alter the fluid properties of TDP-43-positive liquid droplets (Alami et al., 2014; Schmidt and Rohatgi, 2016).

Previous work linking the circadian clock to RBP function provides a foundation for the critical examination of their mechanistic connections in the context of ALS. The role of the lower motor neuron clock in disrupted RBP function and alternative splicing as it relates to ALS disease pathophysiology is not known. Here, we perform transcriptomic analysis of spinal cord cholinergic neurons to elucidate the time-of-day-dependent effects of cell-type-specific clock disruption. We report that the cholinergic neuron rhythmic transcriptome is enriched for genes associated with ALS and other neurodegenerative diseases. We demonstrate that there is circadian regulation of ALS-linked RBPs and rhythmic alternative splicing of genes involved in intracellular transport, microtubule cytoskeleton organization, and synaptic function. Moreover, we establish that the cholinergic neuron clock regulates sporadic ALS (sALS)-associated changes in cytoskeleton and neuromuscular junction (NMJ) synapse gene expression. Finally, we show that cholinergic neuron-specific *Bmal1*-deletion *(i)* increases sciatic nerve axon degeneration, *(ii)* drives alternative splicing of genes encoding ALS-linked RBPs, and *(iii)* drives alternative splicing of genes associated with microtubule transport and postsynaptic organization. Thus, we propose that disruption of the cholinergic neuron circadian clock alters RBP function and contributes to ALS disease phenotypes.

RESULTS

Rhythmic transcriptome profiling of spinal cord cholinergic neurons reveals enrichment for ALS and other neurodegenerative diseases

To elucidate the cholinergic neuron transcriptome, we utilized *ChAT-Cre*;*RiboTag*$^{fx/+}$ mice, which possess a ribosomal hemagglutinin (HA) tag to enable the isolation and characterization of mRNAs specifically bound to cholinergic neuron ribosomes. We isolated RNA from spinal cord cholinergic neurons every 4 hours across the 24-hr day for RNA sequencing (RNA-seq) (Fig. 1A and Fig. S1A-B). We identified 2,391 oscillating transcripts (~12% of genes) by Jonckheere-Terpstra-Kendall (JTK) Cycle analysis and observed that most of the rhythmic transcripts reached maximal abundance at Zeitgeber Time (ZT) 20 and 22 in the dark (active) period, while a smaller cluster of genes was also found to peak at ZT8 in the light (rest) period (Fig. 1B-C; Table S1A). Kyoto Encyclopedia of Genes and Genomes (KEGG) pathway analysis revealed overall enrichment of genes associated with *(i)* neurodegenerative diseases (ALS, Parkinson's disease, Huntington's disease, prion disease, and spinocerebellar ataxia), *(ii)* protein synthesis and degradation (spliceosome, ribosome, protein processing in the endoplasmic reticulum, proteasome, and ubiquitin-mediated proteolysis), *(iii)* metabolism (oxidative phosphorylation, TCA cycle, and metabolic pathways), and *(iv)* synaptic transmission (GABAergic synapse, dopaminergic synapse, and long-term potentiation) (Fig. 1D).

There were 711 rhythmic genes that had peak abundance during the light period (ZT0-12), and Gene Ontology (GO) enrichment analysis revealed over-representation for metabolic and biosynthetic processes, including translation and RNA processing (Fig. S2). In contrast, 1,680 rhythmic genes exhibited peak abundance during the dark period (ZT12-24), and GO analysis revealed enrichment for pathways associated with protein localization and transport (Fig. S2). Notably, we found that 89 of the oscillating transcripts overlapped with KEGG pathway genes associated with ALS, including genes related to oxidative phosphorylation (e.g., *Ndufa5*, *Cox5a*, and *Atp5f1c*), autophagy (e.g., *Sqstm1*, *Atg101*, and *Atg14*), and the oxidative stress response (e.g., *Atf4*, *Pink1*, and *Als2*) (Fig. 1E; Table S1B). Additionally, 15 of the rhythmically expressed ALS genes were associated with the GO term "cytoskeleton organization," including *Pfn1*, *Dctn2*, and *Nefm* (Fig. 1F; Table S1B).

Circadian clock regulates alternative splicing in spinal cord cholinergic neurons

To determine whether alternative pre-mRNA splicing in cholinergic neurons is influenced by circadian time, we used replicate multivariate analysis of transcript splicing (rMATS) to identify alternative splicing events in wild-type (WT) cholinergic neurons collected at 4-hr intervals (Fig. 1A), including skipped exons (SE), mutually exclusive exons (MXE), and alternative 3' and 5' splice sites (A3SS and A5SS). We calculated the percent-spliced in (psi, Ψ) value for all common alternative splicing events in each of the three replicate samples at each time point and performed JTK_Cycle analysis to identify statistically significant oscillations in Ψ. This analysis revealed 11 rhythmic alternative splicing events, consisting of 8 SE, 1 MXE, 1 A3SS, and 1 A5SS (Fig. 2A), with most Ψ values peaking at ZT12 (Fig. 2B; Table S2A-D). Sashimi plots, which illustrate exon inclusion levels by mapping reads across splice junctions, are shown throughout the circadian day to demonstrate rhythmic splicing of *Aftph* (SE), which encodes Aftiphilin, a factor that enables clathrin binding and intracellular transport as part of the AP-1 adaptor complex (Fig. 2C) (Burman et al., 2005). We found that *Aftph* was rhythmically spliced by both SE and A5SS (Fig. 2A; Tables S2A and S2D).

Limch1 and *Drc3* have roles in microtubule and cytoskeleton organization and also displayed rhythmic altered splicing by SE (Fig. 2A; Table S2A). Of note, *Limch1* promotes actin stress fiber assembly and focal adhesion, and alternative splicing of *Limch1* is associated with muscle weakness and calcium-handling deficits (Lin et al., 2017; Penna et al., 2023). Further, Rap GTPase-activating protein (RapGAP) encoding gene *Sipa1l2* regulates synaptic function and vesicle trafficking at presynaptic terminals, and we found that *Sipa1l2* was rhythmically spliced by SE (Fig. 2A; Table S2A) (Andres-Alonso et al., 2019). Two genes exhibited both rhythmic mRNA expression and rhythmic splicing: *Mvb12a*, which regulates vesicle trafficking by enabling ubiquitin and lipid binding, and *Pdcd2l*, which is involved in apoptosis as well as embryonic development (Fig. 2D) (Gao et al., 2022; Tsunematsu et al., 2010). We establish here that genes involved in intracellular transport, cytoskeleton organization, and synaptic function are rhythmically spliced in cholinergic neurons. Notably, a previous report demonstrated that rhythmically spliced genes in pancreatic islets were similarly enriched for trafficking and synaptic regulation (Marcheva et al., 2020).

Because alternative splicing results from interactions between RBPs and splicing regulatory elements in pre-mRNA, we next investigated RBP expression in the cholinergic neuron rhythmic transcriptome. We identified 70 oscillating transcripts that encode splicing-related RBPs (Table S1C), including 5 that overlap with rhythmically expressed ALS

genes—*Fus*, *Hnrnpa2b1*, *Atxn2*, *Taf15*, and *Ncbp1* (Fig. 2E). However, none of the rhythmically expressed RBPs were differentially expressed or differentially spliced in cholinergic neurons with *Bmal1*-loss at ZT8 or ZT20, which suggests that the expression of these RBPs is not directly regulated by the circadian clock. We observed a bimodal distribution in peak phases of mRNA abundance of the oscillating splicing-associated RBPs 12 hours apart at ZT8 and ZT20 (Fig. 2F). While not aligned with the peak phases of RBP expression, peak Ψ values also displayed a bimodal distribution 12 hours apart (at ZT0-2 and ZT12-14) (Fig. 2B). Taken together, these data demonstrate time-of-day-dependent expression of ALS-linked RBPs and establish for the first time that the molecular clock regulates alternative splicing in spinal cord cholinergic neurons.

Cholinergic neuron circadian clock regulates sALS-associated cytoskeleton, ECM, and NMJ gene expression

Given the involvement of the cholinergic neuron clock in neurodegenerative processes, we sought to investigate the transcriptomic consequences of clock disruption through cholinergic neuron-specific deletion of clock activator BMAL1 in the light (ZT8) and dark (ZT20) periods (Fig. 3A and Fig. S1B). We found 48 upregulated genes and 21 downregulated genes in mouse cholinergic neurons with *Bmal1* knockout, or *ChAT-BKO* (*ChAT-Cre;RiboTag*$^{fx/+}$*;Bmal1*$^{fx/fx}$), compared to controls (*ChAT-Cre;RiboTag*$^{fx/+}$) at ZT8 (Fig. 3B; Table S3A). KEGG, GO, and Reactome functional pathway analyses revealed over-representation of genes associated with cell adhesion and movement, cell signaling, development, and Th17 cell differentiation among the upregulated genes, and blood vessel development among the downregulated genes (Fig. 3C). At the opposite phase, we found 74 upregulated genes and 12 downregulated genes in *ChAT-BKO* cholinergic neurons at ZT20 (Fig. 3B; Table S3B). Functional pathway analyses revealed over-representation of genes related to cell adhesion and movement (similar to at ZT8), immune response, and muscle systems among the upregulated genes, and negative regulation of inflammatory response among the downregulated genes (Fig. 3C). Enrichment for circadian rhythms appeared in the up- and down- regulated genes at both time points, as BMAL1 is a component of the core clock molecular feedback loop and its dysregulation influences the abundance of other circadian genes (e.g., *Per2*, *Cry1*, *Cry2*, *Rorc*, *Nr1d1*, and *Nr1d2*) (Table S3C).

Taking a closer look at the genes involved, there were 38 overlapping genes between the differentially expressed genes in *ChAT-BKO* cholinergic neurons at ZT8 and ZT20, including the circadian genes previously mentioned, genes involved in ECM organization (*Col4a2* and *Colq*),

and *Cd24a*, which functions as a cell adhesion molecule and is also involved in immune cell signaling (Fig. 3D). *Cd24a* was rhythmically expressed in WT cholinergic neurons and downregulated with loss of *Bmal1* at both time points, suggesting that it is under direct clock control. Several genes associated with ECM and cytoskeleton organization were upregulated with loss of *Bmal1* at ZT8 (e.g., *Mapk13* and *Serpinh1*) and at ZT20 (e.g., *Tubb6*, *Palld*, and *Loxl4*) (Fig. 3E). The cytoskeleton plays an important role in axonal transport and synaptic integrity, and cytoskeletal defects are prominent in ALS patients and disease models (Clark et al., 2016; Gall et al., 2020). Furthermore, ECM and cytoskeleton crosstalk is crucial for normal cell adhesion and migration processes, and both transcriptomic and proteomic studies have noted dysregulation of ECM biology in ALS samples (Geiger et al., 2001; Lin et al., 2020; Milioto et al., 2024; Qiu et al., 2014). The prevalence of cytoskeleton and ECM-associated genes within the differentially expressed genes in *Bmal1*-deficient cholinergic neurons suggests that clock disruption drives a restructuring that may contribute to deficits in axonal transport, synaptic integrity, and cell adhesion.

At ZT20, deletion of *Bmal1* induced the expression of NMJ genes within the GO term "muscle system process," including *Chrnb4*, *Tpm2*, *Myoz1*, *Ttn*, and *Atp2a1* (Fig. 3F). Moreover, our data revealed an increase in gene expression of the glutamate receptor *N*-methyl-D-aspartate (NMDA) subunit *Grin2c* in *ChAT-BKO* cholinergic neurons at ZT20 along with time-of-day-dependent expression of genes encoding other NMDA subunits (*Grin1*, *Grina*, and *Grin2b*) (Fig. 3G). Lower motor neurons directly innervate skeletal muscle at the NMJ synapse, where they release neurotransmitters that bind to receptors on the muscle fiber to trigger an action potential and muscle contraction (Khalil et al., 2025). In ALS, degeneration of lower motor neurons leads to muscle weakness and atrophy as a result of muscle denervation (Kubat and Picone, 2024). Glutamate is the most abundant excitatory neurotransmitter in the central nervous system (CNS) and glutamate excitotoxicity, or excess glutamate, is linked to motor neuron death in ALS and other neurodegenerative diseases (Bosch et al., 2006; Foran and Trotti, 2009). While acetylcholine is the primary neurotransmitter at mammalian NMJs, glutamate can also be released in a manner that modulates synaptic transmission and plasticity (Brunelli et al., 2005; Colombo and Francolini, 2019; Nishimaru et al., 2005). Previous studies demonstrating circadian regulation of alternative splicing in neurons as well as clock-dependent neurotransmitter release support the idea that there may be clock-mediated RBP regulation of neurotransmitter release at motor neuron NMJ synapses (Gizowski et al., 2016; Marcheva et al., 2020; Shinohara et al., 2002; Wang et al., 2018). Our data indicate that there is circadian

regulation of glutamatergic signaling at the NMJ and suggest that clock disruption during the dark/active period may increase glutamate excitotoxicity.

To further determine whether transcriptomic findings in mouse cholinergic neurons can be translated to humans, we performed in silico analysis of RNA-seq data from ALS patients vs. healthy controls and found that gene expression profiles altered in disease correspond with rhythmic gene networks. In analyzing lumbar spinal cord motor neurons from 13 sALS patients and 8 healthy controls (Krach et al., 2018), we found 1,270 upregulated genes and 318 downregulated genes (Fig. 4A; Table S4A). KEGG, GO, and Reactome functional pathway analyses revealed over-representation of genes associated with ECM, cytoskeleton organization, and immune response among the upregulated genes (Fig. S3A), and enrichment of genes broadly linked to cytoskeleton dynamics and synaptic activation among the downregulated genes (Fig. S3B). Gene set enrichment analysis (GSEA) revealed that the upregulated genes in *ChAT-BKO* mice at both ZT8 and ZT20 tended to be upregulated in sALS patients vs. controls as well (Fig. 4B). Through hypergeometric testing, we found several genes that were significantly upregulated both in *Bmal1* cholinergic neuron knockout mice and sALS patients, including ECM organization genes (*Col4a2* and *Colq*), actin cytoskeleton gene *Palld*, core clock repressor gene *Cry1*, and fatty acid elongation factor *Elovl7* (Fig. 4C; Table S4B).

Importantly, *Colq* is the collagenic tail of acetylcholinesterase (AChE) responsible for anchoring it to the synaptic space of the NMJ (Rotundo, 2003). AChE is an enzyme that breaks down the neurotransmitter acetylcholine, which has been found to be decreased in ALS patients (Campanari et al., 2016). The upregulation of *Colq* in both mouse *ChAT-BKO* neurons and sALS patient lower motor neurons suggests that there may be compensatory induction of this factor following increased degradation of acetylcholine in both clock-disrupted and sALS neurons. Our analysis also revealed upregulation of actin filament stabilization gene *Tpm2* and cytoskeleton-regulating gene *Pla2g7* with *Bmal1*-loss at ZT20 (Lehtinen et al., 2017), and enrichment of these genes among the upregulated genes in sALS patients (Fig. 4D). Finally, we found that 59 of the rhythmic genes in WT mouse cholinergic neurons were significantly enriched among downregulated genes in sALS patients associated with axonal transport (e.g., *Nefl*, *Tuba1a*, and *Mapk8ip3*) and NMJ synaptic regulation (e.g., *Grin2b*, *Atp8a2*, and *Herc1*) (Fig. 4E; Table S4C). Collectively, these findings indicate that there is circadian regulation of sALS-associated processes on the mRNA level and support a role for the cholinergic neuron clock in ALS disease phenotypes.

Cholinergic neuron-specific *Bmal1*-deletion increases sciatic nerve axon degeneration but does not alter mouse metabolic indices

To elucidate the histological changes resulting from cholinergic neuron-specific deletion of *Bmal1*, we performed transmission electron microscopy (TEM) to visualize the sciatic nerve, which enables cholinergic neuron innervation of hindlimb skeletal muscle at the NMJ. In mice with *Bmal1*-loss (*ChAT-Cre;Bmal1*$^{fx/fx}$) compared to controls (*Bmal1*$^{fx/fx}$), we observed an increase in axon degeneration, as characterized by expansion of the myelin sheath and axoplasmic abnormalities, such as shrinkage of the axoplasm (Fig. 5A-D) (Anderson et al., 2016; Essawy et al., 2011; Muzio et al., 2020). Sciatic nerve axon damage is associated with muscle denervation and ALS disease progression (Gordon et al., 2009; Moloney et al., 2014). In line with our transcriptomic analysis of *Bmal1*-deficient cholinergic neurons, we demonstrate morphological changes to sciatic nerve axons that may contribute to altered NMJ dynamics. Circadian behavior includes rhythmic patterns of locomotor activity, respiration, and feeding (Bass and Takahashi, 2010), yet none of these parameters appeared to be altered with cholinergic neuron-specific *Bmal1*-deletion (Fig. S4A-C). Therefore, we postulate that the cellular pathologies of cholinergic neuron clock disruption arise due to cell-autonomous defects. Further, we did not observe changes in mouse whole-animal body or spinal cord weights (Fig. S4D-E).

Cholinergic neuron-specific *Bmal1*-deletion drives alternative splicing of genes encoding ALS-linked RBPs and genes associated with microtubule transport and postsynaptic organization

Since we observed enrichment of differentially expressed genes in *Bmal1* cholinergic neuron knockout mice and sALS patients, we applied rMATS to determine whether these factors likewise undergo alternative splicing. Our analysis of *ChAT-BKO* cholinergic neurons harvested at ZT8 and ZT20 revealed 60 alternative splicing events across 49 unique genes during the light period, consisting of 34 SE, 5 MXE, 12 A3SS, and 9 A5SS (Fig. 6A and 6C; Table S5A-D), and 50 alternative splicing events across 41 unique genes during the dark period, consisting of 37 SE, 1 MXE, 4 A3SS, and 8 A5SS (Fig. 6A and 6C; Table S6A-D). We uncovered differentially spliced genes with multiple transcript variants in *ChAT-BKO* cholinergic neurons, including ALS-associated genes *Stk16* (at ZT8) and *Atg10* (at ZT20), both of which underwent multiple exon skipping events (Fig. 6B) (García-García et al., 2021; Lee et al., 2015; Wang et al., 2019; Zhao et al., 2017). Microtubule-associated protein gene *Ccdc74a* and histone variant encoding gene

H2az2 were the only overlapping alternatively spliced genes between the two time points (Fig. 6C).

Functional pathway analyses of all the genes that were differentially spliced with *ChAT-BKO* at ZT8 revealed enrichment for protein transport, postsynaptic organization, and DNA and RNA stability (Fig. 6D). Notably, deletion of *Bmal1* at ZT8 resulted in altered splicing of several key genes related to microtubule dynamics and transport (*Dync2h1*, *Brsk2*, *Kif3a*, *Tubgcp4*, *Camsap3*, and *Ccdc61*) as well as postsynaptic organization (*Srcin1*, *Arhgef15*, and *Nrcam*) (Fig. 6E). *Kif3a* encodes a subunit of the heterotrimeric KIF3 motor complex, which is crucial for neurite elongation and found to be decreased in sALS patient motor cortex (Hirokawa et al., 2009; Pantelidou et al., 2007). Taken together, this suggests that alternative splicing may alter cytoskeleton and NMJ dynamics during the light/rest period. Intriguingly, the genes that were differentially spliced with *ChAT-BKO* at ZT20 were enriched for a different set of pathways, including RNA splicing, ubiquitin-dependent protein catabolic process, stress response, and purine compound biosynthesis and metabolism (Fig. 6D). This demonstrates that there are time-of-day-dependent differences in clock-mediated regulation of alternative splicing in cholinergic neurons.

An early study comparing sALS lumbar spinal cord motor neurons to healthy controls noted little overlap between the differentially expressed and differentially spliced genes, positing that these cohorts of genes were largely distinct from one another (Rabin et al., 2009). Consistent with this finding, we did not see any overlap between the differentially expressed and differentially spliced genes in *ChAT-BKO* cholinergic neurons at either time point. Moreover, another report found minimal overlap between differentially expressed and differentially spliced genes (0.6% and 4% overlap, respectively) in clock-disrupted pancreatic β-cells (Marcheva et al., 2020). These findings support that changes in splicing and mRNA abundance are regulated by distinct mechanisms that are downstream of the molecular clock.

Of note, our data revealed altered splicing of RBP-encoding genes *Matr3*, *Syncrip*, and *Thoc7* in *ChAT-BKO* cholinergic neurons compared to controls at ZT8, and *Srsf7*, *Snrnp70*, and *U2af2* at ZT20. We found that ALS-linked DNA- and RNA- binding protein *Matr3* was alternatively spliced by SE in cholinergic neurons with *Bmal1*-deletion during the light period, with an increase in exon inclusion levels from 90% to 98% (Fig. 6F). MATR3 is involved in processes such as chromatin organization, RNA processing, and mediating NMDA-induced neuronal cell death, and mutations have been associated with the inhibition of mRNA nuclear export as well as increased cryptic exon inclusion (Boehringer et al., 2017; Giordano et al., 2005;

Johnson et al., 2014b; Khan et al., 2024; Salton et al., 2011). Furthermore, MATR3 has been found to interact with TDP-43, and a subset of sALS patient TDP-43-positive cytoplasmic inclusions were also immunoreactive for MATR3 (Iradi et al., 2018; Tada et al., 2018). Our analysis also revealed that ALS-linked RBP *Srsf7* was alternatively spliced by A5SS in cholinergic neurons with *Bmal1*-deletion during the dark period, with an increase in exon inclusion levels from 72% to 90% (Fig. 6G). SRSF7 is a serine/arginine splicing factor whose depletion was recently found to decrease the abundance of STMN2, which is an ALS-associated microtubule binding protein involved in axon maintenance and regeneration following injury (Klim et al., 2019; Wang et al., 2025).

We establish that there is clock regulation of the splicing of RBPs themselves—including RBPs associated with ALS—and that, because the alternatively spliced RBPs at ZT8 and ZT20 are distinct, this process is time-of-day-dependent. Importantly, we establish that ALS-linked RBPs are rhythmically expressed in WT cholinergic neurons and that, with *Bmal1*-loss, ALS-linked RBPs are differentially expressed and differentially spliced. Given that RBP mutations are a hallmark of ALS and other neurological diseases, it would be interesting to consider how clock-dependent gene expression and splice variants of these RBPs contribute to their own dysregulation as well as their control of alternative splicing in health and disease.

DISCUSSION

Alternative splicing plays a crucial role in the generation of transcriptomic and proteomic diversity, especially in neuronal cell-types, whose complex and specialized functions render them particularly vulnerable to disruption. The circadian clock adds another layer of complexity to this process by modulating post-transcriptional events based on the time-of-day-specific energetic demands of each cell. In addition to elucidating the role of the clock in regulating RBP splice mediators, insight into the spinal cord cholinergic neuron rhythmic transcriptome provides a window into the 24-hr physiological processes occurring within lower motor neurons, the cell-type of ALS disease pathogenesis and fatality. Given the length of motor neuron axons (up to ~1 meter) and the extensive distances RNA cargo have to travel, motor neurons are also uniquely susceptible to disruptions in axonal transport and synaptic transmission. As observed in ALS patients and disease models, this dysregulation often results from disrupted RBP homeostasis.

Mutations in genes encoding a number of RBPs have been linked to ALS. In healthy cells, RBP-bound mRNA is packaged into ribonucleoprotein (RNP) granules that are transported by motor proteins (e.g., dyneins and kinesins) along microtubules to axon terminals for local translation (Maday et al., 2014). Local translation of targeted mRNAs enables the production of specific proteins when and where they are required, such as at synapses, where this process is critical for maintaining synaptic integrity and neurotransmission (Das et al., 2021; Jung et al., 2020). Translation is also mediated by cellular stress, and RBP mutations have been shown to promote the formation of aberrant RNP stress granules, which are membraneless organelles that undergo phase transitions from transient liquid droplets to irreversible, often pathological, solid states (Kiebler and Bassell, 2006; Lin et al., 2015). For example, ALS-linked FUS mutations were found to alter FUS regulation of a motor neuron survival factor SMN and inhibit its transport to axons (Groen et al., 2013) as well as impair RNP granule function by inducing FUS liquid phase transitions (Murakami et al., 2015; Patel et al., 2015). A recent report found that polyglutamine (polyQ) expansions in ATXN2 inhibited mRNA transport and local translation through abnormal sequestration of TDP-43 in RNP granules (Wijegunawardana et al., 2025). Further, ALS-linked mutations in TAF15 were found to increase the number of TAF15-positive axonal and dendritic stress granules (Couthouis et al., 2011), and inhibition of TAF15 methylation resulted in the accumulation of TAF15 in TIA1-positive stress granules (Jobert et al., 2009).

Our investigation into the link between two central evolutionarily conserved processes, the circadian clock transcriptional program and alternative splicing, yields several key findings in the context of ALS pathophysiology. Our data support that disruption of the cholinergic neuron clock alters RBP function and contributes to ALS disease phenotypes, although functional analyses would be needed to inform causal relationships. Notably, our findings reveal an increase in gene expression of the ionotropic glutamate receptor NMDA subunit *Grin2c* in cholinergic neurons with *Bmal1*-loss during the dark/active period along with time-of-day-dependent expression of genes encoding other NMDA subunits (*Grin1*, *Grina*, and *Grin2b*). Glutamate excitotoxicity, or excess release of glutamate and overstimulation of glutamate receptors, is associated with motor neuron death in ALS and other neurodegenerative diseases (Bosch et al., 2006; Foran and Trotti, 2009). Our data propose that *(i)* circadian clock disruption increases glutamate excitotoxicity and *(ii)* there is time-of-day-dependent release and/or uptake of glutamate at the NMJ. These findings may have important implications for the timing and dosage of ALS drugs, such as riluzole, which utilizes sodium channel blockade to inhibit glutamatergic neurotransmission and excitotoxicity (Arnold et al., 2024; Nagoshi et al., 2015).

Environmental disturbances such as jetlag, exposure to artificial light, changes in diet, and mistimed feeding have been shown to disrupt the alignment of the internal clock with the external 24-hr light/dark cycle (Arble et al., 2009; Fonken et al., 2010; Roenneberg et al., 2012). Rhythmic splicing events are also driven by environmental triggers, such as body temperature cycles, which have been shown to stabilize cold-inducible RNA-binding protein (CIRBP) at low ambient temperatures, and drive rhythmic phosphorylation of serine-arginine (SR) proteins to modulate alternative splicing (Gotic et al., 2016; Morf et al., 2012; Preußner et al., 2017). The role of clock disruption and altered RBP function in ALS remains incompletely understood. Future studies should explore whether circadian disruption exacerbates ALS disease phenotypes and how the dysregulation of interconnected circadian and metabolic networks contributes to ALS-associated metabolic changes, both in relation to- and independent of- RBP function (Koletsou and Huppertz, 2025; Ludolph et al., 2023; Nelson and Trotti, 2022). One goal here would be to apply new insight to ALS patient care regimens in which circadian disruption due to environmental factors come into play.

MATERIALS & METHODS

Animals

All animal procedures were conducted in accordance with regulations of the Institutional Animal Care and Use Committee at Northwestern University. All experiments were conducted using C57BL/6J mice maintained on a 12:12 light/dark cycle. WT cholinergic neuron isolation was achieved by crossing *ChAT-Cre* mice (Rossi et al., 2011; JAX #006410; gift from Dr. Loukia Parisiadou at Northwestern University) with *RiboTag*$^{fx/fx}$ mice (Sanz et al., 2009; obtained from Jackson Laboratories #029977) to generate *ChAT-Cre;RiboTag*$^{fx/+}$ mice. These experiments were performed using 10-week-old male mice. Cholinergic neuron-specific deletion of *Bmal1* was achieved by crossing *Bmal1*$^{fx/fx}$ mice (Johnson et al., 2014a) with *ChAT-Cre* or *RiboTag*$^{fx/fx}$ mice to ultimately generate *ChAT-Cre;Bmal1*$^{fx/fx}$ mice (along with *Bmal1*$^{fx/fx}$ littermate controls) and *ChAT-Cre;RiboTag*$^{fx/+}$*;Bmal1*$^{fx/fx}$ mice (along with *ChAT-Cre;RiboTag*$^{fx/+}$ controls). These experiments were performed using 5–7-month-old male mice to assess the added insult of older age on phenotype and transcriptional program.

Activity, feeding, and weight measurements

Mice were individually housed in Promethion Core metabolic cages (Sable Systems International) where they were allowed free access to food and water and acclimated for 4 days prior to data collection. Locomotor activity (measured by beam breaks), RER (measured by the rate of carbon dioxide emission [VCO_2] divided by the rate of oxygen consumption [VO_2]), food intake, and body weight were continuously monitored for 3 days. To obtain spinal cord measurements, fresh spinal cord tissue was isolated, weighed, and normalized to mouse whole-body weight.

Immunohistochemistry

Mice were anesthetized with intraperitoneal injection of Euthasol (390mg/mL pentobarbital sodium, 50mg/mL phenytoin sodium), and then transcardially perfused with phosphate-buffered saline (PBS) followed by 4% paraformaldehyde (PFA) in 0.4M phosphate buffer (pH 7.4). Lumbar spinal cord was isolated, post-fixed in the same fixative overnight at 4°C, and paraffin embedded. 6μm thick sections were cut and mounted onto slides. Samples were then deparaffinized and hydrated prior to antigen retrieval by treatment with Antigen Decloaker (Biocare Medical, CB910M) in a high-pressure chamber for 20 min at 121°C (Deng et al., 2011). For

immunohistochemistry, endogenous peroxidase activity was inhibited using 2% hydrogen peroxide. Samples were blocked for nonspecific binding by incubation with 1% bovine serum albumin in PBS for 1 hr at room temperature, and subsequently incubated with anti-BMAL1 primary antibody in block solution (1:500; Novus Biologicals, NB100-2288) in a humidified chamber overnight at 4°C. Following washes, samples were incubated with Alexa Fluor 594-conjugated donkey anti-rabbit IgG secondary antibody in block solution (1:500; Invitrogen, A21207) in the dark for 1 hr at room temperature. Finally, samples were mounted with ProLong Gold Antifade Mountant (Invitrogen, P36930) and imaged on a DMI4000B confocal microscope (Leica Microsystems).

Transmission electron microscopy and morphometric quantification

Mice were anesthetized with intraperitoneal injection of Euthasol (390mg/mL pentobarbital sodium, 50mg/mL phenytoin sodium), and then transcardially perfused with PBS followed by 4% PFA in 0.4M phosphate buffer (pH 7.4). Sciatic nerve was isolated and immersion-fixed in 0.1M sodium cacodylate buffer (pH 7.35) containing 2.5% glutaraldehyde and 2% PFA overnight at 4°C. Tissue was post-fixed in 2% osmium tetroxide, en bloc stained with 3% uranyl acetate, and dehydrated in ascending grades of ethanol followed by propylene oxide. Samples were then embedded in EMbed 812 Resin (Electron Microscopy Sciences, 14900) and cured overnight in a 60°C oven. 1µm thick sections were cut using the EM UC6 Ultramicrotome (Leica Microsystems) and stained with Toluidine Blue O. Tile stitched images at 40X magnification were acquired using TissueFAXS PLUS (TissueGnostics) to obtain whole nerve cross sections. After images were blinded, severely degenerated axons were counted within each nerve section and divided by the total area of the section (in mm^2). For transmission electron microscopy (TEM), ultrathin 70nm sections were mounted onto mesh copper grids and stained with uranyl acetate and Reynolds Lead Citrate. Images at 1,400X and 2,900X magnification levels were captured at 80 kV using Tecnai G2 Spirit (FEI Company) and Tecnai Imaging & Analysis Software.

Cholinergic neuron ribosome immunoprecipitation and RNA isolation

Spinal cord tissue was isolated and snap-frozen from 10-week-old *ChAT-Cre*;*RiboTag*$^{fx/+}$ mice at ZT0, 4, 8, 12, 16, and 20 or from 6-month-old *ChAT-BKO* (*ChAT-Cre;RiboTag*$^{fx/+}$*;Bmal1*$^{fx/fx}$) mice and controls (*ChAT-Cre;RiboTag*$^{fx/+}$) at ZT8 and ZT20. All samples for each experiment were processed on the same day. Homogenization buffer consisting of 1% sodium deoxycholate, 50mM Tris (pH 7.5), 100mM KCl, 12mM $MgCl_2$, 1% Tergitol (NP-40), 1mM dithiothreitol (DTT),

200U/mL RNasin Ribonuclease Inhibitor (Promega, N2115), 1mg/mL heparin, 100µg/mL cycloheximide, and Protease Inhibitor Cocktail (Sigma-Aldrich, P8340) was made fresh and pre-chilled. One spinal cord was placed in a 2mL Dounce homogenizer vessel on ice with 2mL homogenization buffer, and homogenized with 30 strokes of 'pestle A' followed by 30 strokes of 'pestle B.' The homogenate was then centrifuged at 10,000 RCF for 10 min at 4°C. TRIzol Reagent (Invitrogen, 15596026) was added to 80µL of the spun homogenate and frozen at -80°C as pooled Input (RNA from whole spinal cord). 800µL of the remaining non-pelleted homogenate was incubated with 4µL of anti-HA antibody (BioLegend, 901514) for 4 hours at 4°C with end-over-end rotation. Samples were then incubated with 200µL of pre-washed protein A/G magnetic beads (Thermo Scientific Pierce, 88803) overnight at 4°C with end-over-end rotation. High salt buffer consisting of 50mM Tris (pH 7.5), 300mM KCl, 12mM $MgCl_2$, 1% NP-40, 0.5mM DTT, and 100µg/mL cycloheximide was made fresh and pre-chilled. Samples were placed on a magnetic stand on ice and washed three times with high salt buffer (800µL per wash) to remove non-specific binding from the immunoprecipitate (IP) product. After careful removal of high salt buffer, samples were treated with 700µL of TRIzol Reagent and frozen at -80°C until RNA was extracted using the Direct-zol RNA MicroPrep kit (Zymo Research Corp., R2062) following the manufacturer's instructions.

Quantitative real-time PCR

Following RNA isolation, cDNA was synthesized using the High-Capacity cDNA Reverse Transcription Kit (Applied Biosystems, 4368813). Quantitative real-time PCR (qPCR) was performed with iTaq Universal SYBR Green Supermix (Bio-Rad, 1725124) using a CFX384 Touch Real-Time PCR System (Bio-Rad) and analyzed using Bio-Rad CFX Manager Software (v3.1). PCR conditions were 10 min at 95°C, followed by 35 cycles of 10 sec at 95°C and 15 sec at 60°C. Relative expression levels normalized to *β-actin* were determined using the comparative CT method. All primer sequences are listed in Table S7.

Library preparation and RNA sequencing

Following RNA isolation, RNA quality was assessed by Bioanalyzer (Agilent) and those with an RNA Integrity Number (RIN) greater than 7 were used for library prep. Libraries were constructed from 100 or 300 ng of RNA (for rhythmic or differential analyses, respectively) using the Illumina Stranded mRNA Prep kit (Illumina, 20040534) according to the manufacturer's instructions.

Libraries were quantified by both Bioanalyzer (Agilent) and qPCR-based quantification (Kapa Biosystems). 150bp paired-end sequencing was performed on a NovaSeq X Plus (Illumina) to a minimum depth of 30M reads. Sequences were aligned to the mm10 transcriptome with STAR (v2.7.5) using the –quantMode Transcriptome and GeneCounts options. Gene counts were obtained from mm10 annotations (Ensembl 98) using rsem-calculate-expression (v1.3.0).

Differential expression, differential splicing, and rhythmicity analyses

Differential mRNA expression analysis was performed using DESeq2 (v1.32.0) after removal of genes with < 10 assigned counts. Differentially expressed transcripts were defined as having a false discovery rate (FDR)-adjusted *p*-value < 0.05. Alternative splicing analysis was performed using rMATS (v4.0.2) (Shen et al., 2014) to quantify reads across annotated splice junctions present in the mm10 assembly. Differentially spliced transcripts were defined as having an FDR-adjusted *p*-value < 0.05 and a minimum exon inclusion level difference > 10%. Rhythmic mRNA expression and rhythmic splice frequency throughout the day were assessed by JTK_Cycle analysis (Hughes et al., 2010), allowing for period lengths of 20, 24, or 28 hours to account for 4-hr sampling frequency. Rhythmicity was determined by an FDR-adjusted *p*-value < 0.05. KEGG, GO, and Reactome pathway enrichment analyses were performed using limma and biomaRt (v2.48.2), ShinyGO (v0.77) (Ge et al., 2019), Metascape (Zhou et al., 2019), and Cytoscape (Shannon et al., 2003). Certain plots were made in R (v4.0.3) using ggplot2 (v3.3.0), gplots (v3.1.1), pheatmap (v1.0.12), and fgsea (v1.16.0).

Statistical analysis

Results are presented as mean ± standard error of the mean (SEM). Unless otherwise indicated, statistical analysis was performed by unpaired two-tailed Student's *t*-test. One-way analysis of variance (ANOVA) with Dunnett's correction for multiple comparisons was used for statistical analysis of qPCR data, and two-way ANOVA was used for statistical analysis of activity, RER, and feeding. Hypergeometric tests were used to determine enrichment of genes from one dataset within another. The Wald test with Benjamini-Hochberg correction for multiple comparisons was used for statistical analysis of normalized count data from DESeq2. *P*-values < 0.05 were considered statistically significant. Detailed information on genotype, sample size, and *p*-value can be found within individual figures and figure legends.

ACKNOWLEDGEMENTS

We thank C. Peek and all members of the Kalb and Bass laboratories for helpful discussion. We also thank B. Weidemann for bioinformatics training and L. Reynolds Jr. for TEM assistance. We thank the Northwestern University Center for Genetic Medicine NUSeq Core, Comprehensive Metabolic Core, and Center for Advanced Microscopy (RRID: SCR_020996), supported by NCI CCSG P30 CA060553 awarded to the Robert H. Lurie Comprehensive Cancer Center.

FUNDING

This research was supported by the US Public Health Service NS122908 and NS124802, the US Department of Defense W81XWH-21-1-0236, and the Heather Koster Family Charitable Fund (R.G.K.), NIH T32HL007909 and the Northwestern University Center for Sleep and Circadian Biology (S.B.T.), and the Les Turner ALS Foundation (R.G.K., S.B.T., E.M.B., E.K., and M.W.). E.K. is a New York Stem Cell Foundation – Robertson Investigator.

AUTHOR CONTRIBUTIONS

S.B.T. performed and analyzed all experiments with assistance from N.J.W., M.W., and E.M.B.; S.B.T., R.G.K., and J.B. wrote and edited the manuscript.

COMPETING INTERESTS

The authors declare no competing financial interests.

FIGURE LEGENDS

Figure 1. Rhythmic transcriptome profiling of spinal cord cholinergic neurons reveals enrichment for ALS and other neurodegenerative diseases. **(A)** Schematic showing RNA isolation in spinal cord cholinergic neurons from *ChAT-Cre*;*RiboTag*$^{fx/+}$ mice every 4 hours across the 24-hr day (ZT0, 4, 8, 12, 16, and 20) for RNA-seq. Created using BioRender. **(B)** Heatmap showing rhythmic cholinergic neuron mRNA expression (n = 3 per time point). **(C)** Radial histogram showing the number of oscillating genes that have peak expression within each 2-hr window. **(D)** KEGG pathway analysis of all oscillating genes in cholinergic neurons. See also Figure S2. **(E)** Overlap of rhythmic transcripts and KEGG pathway ALS genes. **(F)** Examples of time-of-day-dependent expression of ALS-linked genes that regulate cytoskeleton dynamics, shown as normalized counts identified through DESeq2 (n = 3 per time point). Data are represented as mean ± SEM. Rhythmicity was determined by JTK_Cycle analysis (adjusted p-value shown).

Figure 2. Circadian clock regulates alternative splicing in spinal cord cholinergic neurons. **(A)** Heatmap showing rhythmically spliced genes in WT cholinergic neurons obtained using rMATS splicing analysis, represented as splice frequency (Ψ) relative to ZT0 (n = 3 per time point). **(B)** Radial histogram showing the number of each type of splicing event with peak Ψ occurring within each 2-hr window. Radius corresponds to 4 splicing events. SE, skipped exon; MXE, mutually exclusive exon; A3SS and A5SS, alternative 3' and 5' splice sites. **(C)** Sashimi plots showing time-of-day-dependent alternative splicing of *Aftph* by SE every 4 hours across the 24-hr day, with the exon inclusion level indicated at each time point. **(D)** Rhythmic splicing graphs of the genes that are both rhythmically expressed and rhythmically spliced in WT cholinergic neurons (n = 3 per time point). Data are represented as mean ± SEM and double-plotted for better visualization. Rhythmicity was determined by JTK_Cycle analysis (adjusted p-value < 0.05). **(E)** Overlap of rhythmically expressed ALS genes and genes that encode RNA-binding proteins (RBPs). **(F)** Peak phase in expression of oscillating RBPs within the GO term "RNA splicing."

Figure 3. Cholinergic neuron circadian clock regulates cytoskeleton, ECM, and NMJ gene expression. **(A)** Model of cholinergic neuron-specific deletion of BMAL1 during the light (ZT8) and dark (ZT20) periods to induce the expression of cytoskeleton, extracellular matrix (ECM), and neuromuscular junction (NMJ) genes. Created using BioRender. **(B)** Heatmaps showing differentially expressed genes between cholinergic neurons isolated from control (*ChAT-*

Cre;RiboTag$^{fx/+}$) and *ChAT-BKO* (*ChAT-Cre;RiboTag*$^{fx/+}$*;Bmal1*$^{fx/fx}$) mice at ZT8 and ZT20 (n = 6 per condition). **(C)** KEGG, GO, and Reactome functional pathway analyses of genes that are up- or down- regulated in *ChAT-BKO* cholinergic neurons vs. controls at ZT8 and ZT20. **(D)** Overlap of differentially expressed genes in *ChAT-BKO* cholinergic neurons at ZT8 and ZT20. **(E)** Increased expression of GO or literature-defined genes associated with cytoskeleton organization and ECM in *ChAT-BKO* cholinergic neurons at ZT8 and ZT20. **(F)** Volcano plot showing induction of NMJ genes within the GO term "Muscle system process" in *ChAT-BKO* cholinergic neurons at ZT20. **(G)** Induction of glutamate receptor NMDA subunit *Grin2c* in *ChAT-BKO* cholinergic neurons at ZT20 (n = 6 per condition) and time-of-day-dependent expression of genes encoding other NMDA subunits (n = 3 per time point), shown as normalized counts identified through DESeq2. Data are represented as mean ± SEM. Statistical significance was calculated using the Wald test with Benjamini-Hochberg correction for multiple comparisons (*adjusted $p < 0.05$) and rhythmicity was determined by JTK_Cycle analysis (adjusted p-value shown).

Figure 4. Cholinergic neuron circadian clock regulates sALS-associated cytoskeleton, ECM, and NMJ gene expression. **(A)** Volcano plot showing differentially expressed genes between sporadic ALS (sALS) patient lumbar spinal cord motor neurons (n = 13) and healthy controls (n = 8). Re-analysis of data set from Krach et al., 2018. See also Figure S3. **(B)** GSEA plots showing enrichment of upregulated genes in *ChAT-BKO* (*ChAT-Cre;RiboTag*$^{fx/+}$*;Bmal1*$^{fx/fx}$) mouse cholinergic neurons vs. controls (*ChAT-Cre;RiboTag*$^{fx/+}$) at ZT8 and ZT20 [data from Figure 3] among rank-ordered genes in sALS patient motor neurons vs. controls (normalized enrichment score [NES] and false discovery rate [FDR]-adjusted p-value shown). **(C)** Upregulated genes in *ChAT-BKO* mice at ZT8 and ZT20 that are over-represented among upregulated genes in sALS patients (adjusted $p < 0.01$ in hypergeometric tests at both time points). **(D)** Volcano plot of upregulated genes in *ChAT-BKO* mice at ZT20 that are over-represented among upregulated genes in sALS patients. **(E)** Enrichment of rhythmic genes in WT mouse cholinergic neurons among sALS patient downregulated genes involved in axonal transport and NMJ (adjusted $p < 0.01$ in hypergeometric test).

Figure 5. Cholinergic neuron-specific *Bmal1*-deletion increases axon degeneration in sciatic nerve. **(A and B)** Representative images of toluidine blue-stained sciatic nerve sections from control *Bmal1*$^{fx/fx}$ mice (A) and *ChAT-Cre;Bmal1*$^{fx/fx}$ mice (B). Scale bars represent 100μm and

25μm (magnified view). **(C)** Transmission electron microscopy (TEM) images of degenerated axons shown in (B). Scale bars represent 5μm and 2μm (magnified view). **(D)** Quantification of degenerated axons per sciatic nerve section (measured in mm^2) in *ChAT-Cre;Bmal1*$^{fx/fx}$ vs. control mice (n = 5-6). Data are represented as mean ± SEM. Statistical significance was calculated by unpaired two-tailed Student's *t*-test (*p < 0.05, **p < 0.01).

Figure 6. Cholinergic neuron-specific *Bmal1*-deletion drives alternative splicing of genes encoding ALS-linked RBPs and genes associated with microtubule transport and postsynaptic organization. **(A)** Alternative splicing events in *ChAT-BKO* (*ChAT-Cre;RiboTag*$^{fx/+}$*;Bmal1*$^{fx/fx}$) cholinergic neurons vs. controls (*ChAT-Cre;RiboTag*$^{fx/+}$) at ZT8 and ZT20 determined by rMATS analysis (n = 6 per condition). SE, skipped exon; MXE, mutually exclusive exon; A3SS and A5SS, alternative 3' and 5' splice sites. **(B)** Differentially spliced genes with multiple transcript variants in *ChAT-BKO* cholinergic neurons at ZT8 and ZT20. **(C)** Overlap of alternatively spliced genes in *ChAT-BKO* cholinergic neurons at ZT8 and ZT20. **(D)** KEGG, GO, and Reactome functional pathway analyses of alternatively spliced genes in *ChAT-BKO* cholinergic neurons at ZT8 and ZT20. **(E)** Volcano plots of alternatively spliced genes by SE, MXE, A3SS, and A5SS in *ChAT-BKO* cholinergic neurons at ZT8, including several associated with microtubule dynamics and postsynaptic organization. **(F and G)** Sashimi plots showing altered splicing of ALS-linked RBPs *Matr3* by SE in *ChAT-BKO* cholinergic neurons at ZT8 (F) and *Srsf7* by A5SS in *ChAT-BKO* cholinergic neurons at ZT20 (G), with exon inclusion levels indicated.

Figure S1. Confirmation of cholinergic neuron isolation and *Bmal1*-deletion. **(A)** Cholinergic neuron enrichment in *ChAT-Cre*;*RiboTag*$^{fx/+}$ mouse spinal cord IP product, as assessed by qPCR (n = 3). Data are represented as mean ± SEM. Statistical significance was calculated by one-way ANOVA with Dunnett's correction for multiple comparisons (*p < 0.05, **p < 0.01, ***p < 0.001, ****p < 0.0001). **(B)** Representative immunofluorescence staining of BMAL1 (red) in *Bmal1*$^{fx/fx}$ and *ChAT-Cre;Bmal1*$^{fx/fx}$ lumbar spinal cord tissue sections. Scale bar represents 100μm.

Figure S2. GO enrichment analysis of oscillating genes in cholinergic neurons with peak expression during the light (ZT0-12) and dark (ZT12-24) periods (n = 3 per time point).

Figure S3. Pathway enrichment analyses of differentially expressed genes between sALS patients and healthy controls. **(A)** KEGG, GO, and Reactome functional pathway analyses of genes that are upregulated in sALS patient lumbar spinal cord motor neurons vs. healthy controls. **(B)** Network interconnection map showing functional pathway enrichment of genes that are downregulated in sALS patient lumbar spinal cord motor neurons vs. healthy controls. Circle nodes are color-coordinated by cluster identity. The size of each node is proportional to the number of genes within a given term. Terms with a similarity score > 0.3 are linked by an edge, with thicker edges reflecting higher similarity scores (n = 13 sALS patients and 8 healthy controls). Re-analysis of data set from Krach et al., 2018.

Figure S4. Cholinergic neuron-specific *Bmal1*-deletion does not alter activity or RER rhythms, food intake, or weight. **(A and B)** Activity rhythms and total activity over 12 hours (A) and respiratory exchange ratio (RER) rhythms and average RER over 12 hours (B) in control *Bmal1*$^{fx/fx}$ and *ChAT-Cre;Bmal1*$^{fx/fx}$ mice recorded over 3 days. The shaded regions denote the dark (active) time periods. **(C)** Cumulative food intake within each 12-hr period over 3 days. **(D)** Average body weight over 3 days (n = 5-7 for [A-D]). **(E)** Weight of isolated spinal cords as a percentage of total body weight (n = 9-10). Data are represented as mean ± SEM. Statistical significance was calculated by two-way ANOVA, with no differences between experimental and control groups within each 12-hr period and $p < 0.0001$ for all comparisons between light (ZT0-12) and dark (ZT12-24) periods ([A-C]), or unpaired two-tailed Student's *t*-test (D and E).

REFERENCES

Alami NH, Smith RB, Carrasco MA, Williams LA, Winborn CS, Han SSW, Kiskinis E, Winborn B, Freibaum BD, Kanagaraj A, et al. 2014. Axonal transport of TDP-43 mRNA granules is impaired by ALS-causing mutations. Neuron. 81:536-543. doi: 10.1016/j.neuron.2013.12.018. PMID: 24507191; PMCID: PMC3939050.

Anderson DM, Cannavino J, Li H, Anderson KM, Nelson BR, McAnally J, Bezprozvannaya S, Liu Y, Lin W, Liu N, et al. 2016. Severe muscle wasting and denervation in mice lacking the RNA-binding protein ZFP106. Proc Natl Acad Sci U S A. 113:E4494-4503. doi: 10.1073/pnas.1608423113. PMID: 27418600; PMCID: PMC4978283.

Andres-Alonso M, Ammar MR, Butnaru I, Gomes GM, Acuña Sanhueza G, Raman R, Yuanxiang P, Borgmeyer M, Lopez-Rojas J, Raza SA, et al. 2019. SIPA1L2 controls trafficking and local signaling of TrkB-containing amphisomes at presynaptic terminals. Nat Commun. 10:5448. doi: 10.1038/s41467-019-13224-z. PMID: 31784514; PMCID: PMC6884526.

Arble DM, Bass J, Laposky AD, Vitaterna MH, Turek FW. 2009. Circadian timing of food intake contributes to weight gain. Obesity (Silver Spring). 17:2100-2102. doi: 10.1038/oby.2009.264. PMID: 19730426; PMCID: PMC3499064.

Arnold FJ, Putka AF, Raychaudhuri U, Hsu S, Bedlack RS, Bennett CL, La Spada AR. 2024. Revisiting Glutamate Excitotoxicity in Amyotrophic Lateral Sclerosis and Age-Related Neurodegeneration. Int J Mol Sci. 25:5587. doi: 10.3390/ijms25115587. PMID: 38891774; PMCID: PMC11171854.

Bass J, Takahashi JS. 2010. Circadian integration of metabolism and energetics. Science. 330:1349-1354. doi: 10.1126/science.1195027. PMID: 21127246; PMCID: PMC3756146.

Bass J. 2012. Circadian topology of metabolism. Nature. 491:348-356. doi: 10.1038/nature11704. PMID: 23151577.

Boehringer A, Garcia-Mansfield K, Singh G, Bakkar N, Pirrotte P, Bowser R. 2017. ALS Associated Mutations in Matrin 3 Alter Protein-Protein Interactions and Impede mRNA Nuclear Export. Sci Rep. 7:14529. doi: 10.1038/s41598-017-14924-6. PMID: 29109432; PMCID: PMC5674072.

Brunelli G, Spano P, Barlati S, Guarneri B, Barbon A, Bresciani R, Pizzi M. 2005. Glutamatergic reinnervation through peripheral nerve graft dictates assembly of glutamatergic synapses at rat skeletal muscle. Proc Natl Acad Sci U S A. 102:8752-8757. doi: 10.1073/pnas.0500530102. PMID: 15937120; PMCID: PMC1142481.

Burman JL, Wasiak S, Ritter B, de Heuvel E, McPherson PS. 2005. Aftiphilin is a component of the clathrin machinery in neurons. FEBS Lett. 579:2177-2184. doi: 10.1016/j.febslet.2005.03.008. PMID: 15811338.

Campanari ML, García-Ayllón MS, Ciura S, Sáez-Valero J, Kabashi E. 2016. Neuromuscular Junction Impairment in Amyotrophic Lateral Sclerosis: Reassessing the Role of

Acetylcholinesterase. Front Mol Neurosci. 9:160. doi: 10.3389/fnmol.2016.00160. PMID: 28082868; PMCID: PMC5187284.

Chen M, Manley JL. 2009. Mechanisms of alternative splicing regulation: insights from molecular and genomics approaches. Nat Rev Mol Cell Biol. 10:741-754. doi: 10.1038/nrm2777. PMID: 19773805; PMCID: PMC2958924.

Clark JA, Yeaman EJ, Blizzard CA, Chuckowree JA, Dickson TC. 2016. A Case for Microtubule Vulnerability in Amyotrophic Lateral Sclerosis: Altered Dynamics During Disease. Front Cell Neurosci. 10:204. doi: 10.3389/fncel.2016.00204. PMID: 27679561; PMCID: PMC5020100.

Colombo MN, Francolini M. 2019. Glutamate at the Vertebrate Neuromuscular Junction: From Modulation to Neurotransmission. Cells. 8:996. doi: 10.3390/cells8090996. PMID: 31466388; PMCID: PMC6770210.

Couthouis J, Hart MP, Shorter J, DeJesus-Hernandez M, Erion R, Oristano R, Liu AX, Ramos D, Jethava N, Hosangadi D, et al. 2011. A yeast functional screen predicts new candidate ALS disease genes. Proc Natl Acad Sci U S A. 108:20881-20890. doi: 10.1073/pnas.1109434108. Erratum in: Proc Natl Acad Sci U S A. 2023. 120:e2220845120. doi: 10.1073/pnas.2220845120. PMID: 22065782; PMCID: PMC3248518.

Das S, Vera M, Gandin V, Singer RH, Tutucci E. 2021. Intracellular mRNA transport and localized translation. Nat Rev Mol Cell Biol. 22:483-504. doi: 10.1038/s41580-021-00356-8. Erratum in: Nat Rev Mol Cell Biol. 2021. 22:505. doi: 10.1038/s41580-021-00374-6. PMID: 33837370; PMCID: PMC9346928.

Deng HX, Bigio EH, Siddique T. 2011. Detection of protein aggregation in neurodegenerative diseases. Methods Mol Biol. 793:259-272. doi: 10.1007/978-1-61779-328-8_17. PMID: 21913106.

Essawy AE, Abdel-Moneim AM, Gaaboub IA, El-Sayed SA. 2011. Adverse effects of dimethyl disulphide on sciatic nerve of Swiss albino mice. Afr J Biotechnol. 10:11081-11086.

Fonken LK, Workman JL, Walton JC, Weil ZM, Morris JS, Haim A, Nelson RJ. 2010. Light at night increases body mass by shifting the time of food intake. Proc Natl Acad Sci U S A. 107:18664-18669. doi: 10.1073/pnas.1008734107. PMID: 20937863; PMCID: PMC2972983.

Foran E, Trotti D. 2009. Glutamate transporters and the excitotoxic path to motor neuron degeneration in amyotrophic lateral sclerosis. Antioxid Redox Signal. 11:1587-1602. doi: 10.1089/ars.2009.2444. PMID: 19413484; PMCID: PMC2842587.

Freibaum BD, Chitta RK, High AA, Taylor JP. 2010. Global analysis of TDP-43 interacting proteins reveals strong association with RNA splicing and translation machinery. J Proteome Res. 9:1104-1120. doi: 10.1021/pr901076y. PMID: 20020773; PMCID: PMC2897173.

Fustin JM, Doi M, Yamaguchi Y, Hida H, Nishimura S, Yoshida M, Isagawa T, Morioka MS, Kakeya H, Manabe I, et al. 2013. RNA-methylation-dependent RNA processing controls the speed of the circadian clock. Cell. 155:793-806. doi: 10.1016/j.cell.2013.10.026. PMID: 24209618.

Gao H, Xu C, Liang J, Ge S, Zhang F, Tuo Y, Shi H, Han A. 2022. Pan-cancer analysis of oncogenic role of Programmed Cell Death 2 Like (PDCD2L) and validation in colorectal cancer. Cancer Cell Int. 22:100. doi: 10.1186/s12935-022-02525-x. PMID: 35216602; PMCID: PMC8881831.

García-García R, Martín-Herrero L, Blanca-Pariente L, Pérez-Cabello J, Roodveldt C. 2021. Immune Signaling Kinases in Amyotrophic Lateral Sclerosis (ALS) and Frontotemporal Dementia (FTD). Int J Mol Sci. 22:13280. doi: 10.3390/ijms222413280. PMID: 34948077; PMCID: PMC8707599.

Ge SX, Jung D, Yao R. 2020. ShinyGO: a graphical gene-set enrichment tool for animals and plants. Bioinformatics. 36:2628-2629. doi: 10.1093/bioinformatics/btz931. PMID: 31882993; PMCID: PMC7178415.

Geiger B, Bershadsky A, Pankov R, Yamada KM. 2001. Transmembrane crosstalk between the extracellular matrix--cytoskeleton crosstalk. Nat Rev Mol Cell Biol. 2:793-805. doi: 10.1038/35099066. PMID: 11715046.

Giordano G, Sánchez-Pérez AM, Montoliu C, Berezney R, Malyavantham K, Costa LG, Calvete JJ, Felipo V. 2005. Activation of NMDA receptors induces protein kinase A-mediated phosphorylation and degradation of matrin 3. Blocking these effects prevents NMDA-induced neuronal death. J Neurochem. 94:808-818. doi: 10.1111/j.1471-4159.2005.03235.x. PMID: 16000164.

Gizowski C, Zaelzer C, Bourque CW. 2016. Clock-driven vasopressin neurotransmission mediates anticipatory thirst prior to sleep. Nature. 537:685-688. doi: 10.1038/nature19756. PMID: 27680940.

Gordon T, Ly V, Hegedus J, Tyreman N. 2009. Early detection of denervated muscle fibers in hindlimb muscles after sciatic nerve transection in wild type mice and in the G93A mouse model of amyotrophic lateral sclerosis. Neurol Res. 31:28-42. doi: 10.1179/174313208X332977. PMID: 18768111.

Gotic I, Omidi S, Fleury-Olela F, Molina N, Naef F, Schibler U. 2016. Temperature regulates splicing efficiency of the cold-inducible RNA-binding protein gene Cirbp. Genes Dev. 30:2005-2017. doi: 10.1101/gad.287094.116. PMID: 27633015; PMCID: PMC5066242.

Green CB. 2018. Circadian Posttranscriptional Regulatory Mechanisms in Mammals. Cold Spring Harb Perspect Biol. 10:a030692. doi: 10.1101/cshperspect.a030692. PMID: 28778869; PMCID: PMC5983185.

Groen EJ, Fumoto K, Blokhuis AM, Engelen-Lee J, Zhou Y, van den Heuvel DM, Koppers M, van Diggelen F, van Heest J, Demmers JA, et al. 2013. ALS-associated mutations in FUS disrupt the axonal distribution and function of SMN. Hum Mol Genet. 22:3690-3704. doi: 10.1093/hmg/ddt222. PMID: 23681068.

Hirokawa N, Noda Y, Tanaka Y, Niwa S. 2009. Kinesin superfamily motor proteins and intracellular transport. Nat Rev Mol Cell Biol. 10:682-696. doi: 10.1038/nrm2774. PMID: 19773780.

Hughes ME, Hogenesch JB, Kornacker K. 2010. JTK_CYCLE: an efficient nonparametric algorithm for detecting rhythmic components in genome-scale data sets. J Biol Rhythms. 25:372-380. doi: 10.1177/0748730410379711. PMID: 20876817; PMCID: PMC3119870.

Hughes ME, Grant GR, Paquin C, Qian J, Nitabach MN. 2012. Deep sequencing the circadian and diurnal transcriptome of Drosophila brain. Genome Res. 22:1266-1281. doi: 10.1101/gr.128876.111. PMID: 22472103; PMCID: PMC3396368.

Iradi MCG, Triplett JC, Thomas JD, Davila R, Crown AM, Brown H, Lewis J, Swanson MS, Xu G, Rodriguez-Lebron E, et al. 2018. Characterization of gene regulation and protein interaction networks for Matrin 3 encoding mutations linked to amyotrophic lateral sclerosis and myopathy. Sci Rep. 8:4049. doi: 10.1038/s41598-018-21371-4. PMID: 29511296; PMCID: PMC5840295.

Jobert L, Argentini M, Tora L. 2009. PRMT1 mediated methylation of TAF15 is required for its positive gene regulatory function. Exp Cell Res. 315:1273-1286. doi: 10.1016/j.yexcr.2008.12.008. PMID: 19124016.

Johnson BP, Walisser JA, Liu Y, Shen AL, McDearmon EL, Moran SM, McIntosh BE, Vollrath AL, Schook AC, Takahashi JS, et al. 2014. Hepatocyte circadian clock controls acetaminophen bioactivation through NADPH-cytochrome P450 oxidoreductase. Proc Natl Acad Sci U S A. 111:18757-18762. doi: 10.1073/pnas.1421708111. PMID: 25512522; PMCID: PMC4284582.

Johnson JO, Pioro EP, Boehringer A, Chia R, Feit H, Renton AE, Pliner HA, Abramzon Y, Marangi G, Winborn BJ, et al. 2014. Mutations in the Matrin 3 gene cause familial amyotrophic lateral sclerosis. Nat Neurosci. 17:664-666. doi: 10.1038/nn.3688. PMID: 24686783; PMCID: PMC4000579.

Jung Y, Seo JY, Ryu HG, Kim DY, Lee KH, Kim KT. 2020. BDNF-induced local translation of *GluA1* is regulated by HNRNP A2/B1. Sci Adv. 6:eabd2163. doi: 10.1126/sciadv.abd2163. PMID: 33219033; PMCID: PMC7679154.

Kapeli K, Martinez FJ, Yeo GW. 2017. Genetic mutations in RNA-binding proteins and their roles in ALS. Hum Genet. 136:1193-1214. doi: 10.1007/s00439-017-1830-7. PMID: 28762175; PMCID: PMC5602095.

Khalil B, Marwaha K, Bollu PC. Physiology, Neuromuscular Junction. Updated 2025 Feb 17. In: StatPearls. Treasure Island (FL): StatPearls Publishing; Available from: https://www.ncbi.nlm.nih.gov/books/NBK470413/.

Khan M, Chen XXL, Dias M, Santos JR, Kour S, You J, van Bruggen R, Youssef MMM, Wan YW, Liu Z, et al. 2024. MATR3 pathogenic variants differentially impair its cryptic splicing repression function. FEBS Lett. 598:415-436. doi: 10.1002/1873-3468.14806. PMID: 38320753.

Kiebler MA, Bassell GJ. 2006. Neuronal RNA granules: movers and makers. Neuron. 51:685-690. doi: 10.1016/j.neuron.2006.08.021. PMID: 16982415.

Klim JR, Williams LA, Limone F, Guerra San Juan I, Davis-Dusenbery BN, Mordes DA, Burberry A, Steinbaugh MJ, Gamage KK, Kirchner R, et al. 2019. ALS-implicated protein TDP-43 sustains levels of STMN2, a mediator of motor neuron growth and repair. Nat Neurosci. 22:167-179. doi: 10.1038/s41593-018-0300-4. PMID: 30643292; PMCID: PMC7153761.

Koike N, Yoo SH, Huang HC, Kumar V, Lee C, Kim TK, Takahashi JS. 2012. Transcriptional architecture and chromatin landscape of the core circadian clock in mammals. Science. 338:349-354. doi: 10.1126/science.1226339. PMID: 22936566; PMCID: PMC3694775.

Kojima S, Shingle DL, Green CB. 2011. Post-transcriptional control of circadian rhythms. J Cell Sci. 124:311-320. doi: 10.1242/jcs.065771. PMID: 21242310; PMCID: PMC3021995.

Kojima S, Sher-Chen EL, Green CB. 2012. Circadian control of mRNA polyadenylation dynamics regulates rhythmic protein expression. Genes Dev. 26:2724-2736. doi: 10.1101/gad.208306.112. PMID: 23249735; PMCID: PMC3533077.

Koletsou E, Huppertz I. 2025. RNA-binding proteins as versatile metabolic regulators. npj Metab Health Dis. 3:1. doi: 10.1038/s44324-024-00044-z.

Krach F, Batra R, Wheeler EC, Vu AQ, Wang R, Hutt K, Rabin SJ, Baughn MW, Libby RT, Diaz-Garcia S, et al. 2018. Transcriptome-pathology correlation identifies interplay between TDP-43 and the expression of its kinase CK1E in sporadic ALS. Acta Neuropathol. 136:405-423. doi: 10.1007/s00401-018-1870-7. PMID: 29881994; PMCID: PMC6215775.

Kubat GB, Picone P. 2024. Skeletal muscle dysfunction in amyotrophic lateral sclerosis: a mitochondrial perspective and therapeutic approaches. Neurol Sci. 45:4121-4131. doi: 10.1007/s10072-024-07508-6. PMID: 38676818; PMCID: PMC11306305.

Le Gall L, Anakor E, Connolly O, Vijayakumar UG, Duddy WJ, Duguez S. 2020. Molecular and Cellular Mechanisms Affected in ALS. J Pers Med. 10:101. doi: 10.3390/jpm10030101. PMID: 32854276; PMCID: PMC7564998.

Lee JK, Shin JH, Lee JE, Choi EJ. 2015. Role of autophagy in the pathogenesis of amyotrophic lateral sclerosis. Biochim Biophys Acta. 1852:2517-2524. doi: 10.1016/j.bbadis.2015.08.005. PMID: 26264610.

Lehtinen L, Vainio P, Wikman H, Huhtala H, Mueller V, Kallioniemi A, Pantel K, Kronqvist P, Kallioniemi O, Carpèn O, et al. 2017. *PLA2G7* associates with hormone receptor negativity in clinical breast cancer samples and regulates epithelial-mesenchymal transition in cultured breast cancer cells. J Pathol Clin Res. 3:123-138. doi: 10.1002/cjp2.69. PMID: 28451461; PMCID: PMC5402179.

Lin J, Huang P, Chen W, Ye C, Su H, Yao X. 2020. Key Molecules and Pathways Underlying Sporadic Amyotrophic Lateral Sclerosis: Integrated Analysis on Gene Expression Profiles of Motor Neurons. Front Genet. 11:578143. doi: 10.3389/fgene.2020.578143. PMID: 33240324; PMCID: PMC7680998.

Lin Y, Protter DS, Rosen MK, Parker R. 2015. Formation and Maturation of Phase-Separated Liquid Droplets by RNA-Binding Proteins. Mol Cell. 60:208-219. doi: 10.1016/j.molcel.2015.08.018. PMID: 26412307; PMCID: PMC4609299.

Lin YH, Zhen YY, Chien KY, Lee IC, Lin WC, Chen MY, Pai LM. 2017. LIMCH1 regulates nonmuscle myosin-II activity and suppresses cell migration. Mol Biol Cell. 28:1054-1065. doi: 10.1091/mbc.E15-04-0218. PMID: 28228547; PMCID: PMC5391182.

Lowrey PL, Takahashi JS. 2004. Mammalian circadian biology: elucidating genome-wide levels of temporal organization. Annu Rev Genomics Hum Genet. 5:407-441. doi: 10.1146/annurev.genom.5.061903.175925. PMID: 15485355; PMCID: PMC3770722.

Ludolph A, Dupuis L, Kasarskis E, Steyn F, Ngo S, McDermott C. 2023. Nutritional and metabolic factors in amyotrophic lateral sclerosis. Nat Rev Neurol. 19:511-524. doi: 10.1038/s41582-023-00845-8. PMID: 37500993.

Maday S, Twelvetrees AE, Moughamian AJ, Holzbaur EL. 2014. Axonal transport: cargo-specific mechanisms of motility and regulation. Neuron. 84:292-309. doi: 10.1016/j.neuron.2014.10.019. PMID: 25374356; PMCID: PMC4269290.

Marcheva B, Perelis M, Weidemann BJ, Taguchi A, Lin H, Omura C, Kobayashi Y, Newman MV, Wyatt EJ, McNally EM, et al. 2020. A role for alternative splicing in circadian control of exocytosis and glucose homeostasis. Genes Dev. 34:1089-1105. doi: 10.1101/gad.338178.120. PMID: 32616519; PMCID: PMC7397853. Erratum in: Genes Dev. 2021. 35:425. doi: 10.1101/gad.348303.121. PMID: 32616519; PMCID: PMC7397853.

McGlincy NJ, Valomon A, Chesham JE, Maywood ES, Hastings MH, Ule J. 2012. Regulation of alternative splicing by the circadian clock and food related cues. Genome Biol. 13:R54. doi: 10.1186/gb-2012-13-6-r54. PMID: 22721557; PMCID: PMC3446320.

Menet JS, Rodriguez J, Abruzzi KC, Rosbash M. 2012. Nascent-Seq reveals novel features of mouse circadian transcriptional regulation. Elife. 1:e00011. doi: 10.7554/eLife.00011. PMID: 23150795; PMCID: PMC3492862.

Milioto C, Carcolé M, Giblin A, Coneys R, Attrebi O, Ahmed M, Harris SS, Lee BI, Yang M, Ellingford RA, et al. 2024. PolyGR and polyPR knock-in mice reveal a conserved neuroprotective extracellular matrix signature in C9orf72 ALS/FTD neurons. Nat Neurosci. 27:643-655. doi: 10.1038/s41593-024-01589-4. PMID: 38424324; PMCID: PMC11001582.

Moloney EB, de Winter F, Verhaagen J. 2014. ALS as a distal axonopathy: molecular mechanisms affecting neuromuscular junction stability in the presymptomatic stages of the disease. Front Neurosci. 8:252. doi: 10.3389/fnins.2014.00252. PMID: 25177267; PMCID: PMC4132373.

Morf J, Rey G, Schneider K, Stratmann M, Fujita J, Naef F, Schibler U. 2012. Cold-inducible RNA-binding protein modulates circadian gene expression posttranscriptionally. Science. 338:379-383. doi: 10.1126/science.1217726. PMID: 22923437.

Murakami T, Qamar S, Lin JQ, Schierle GS, Rees E, Miyashita A, Costa AR, Dodd RB, Chan FT, Michel CH, et al. 2015. ALS/FTD Mutation-Induced Phase Transition of FUS Liquid Droplets and Reversible Hydrogels into Irreversible Hydrogels Impairs RNP Granule Function. Neuron. 88:678-690. doi: 10.1016/j.neuron.2015.10.030. PMID: 26526393; PMCID: PMC4660210.

Muzio L, Sirtori R, Gornati D, Eleuteri S, Fossaghi A, Brancaccio D, Manzoni L, Ottoboni L, Feo L, Quattrini A, et al. 2020. Retromer stabilization results in neuroprotection in a model of Amyotrophic Lateral Sclerosis. Nat Commun. 11:3848. doi: 10.1038/s41467-020-17524-7. PMID: 32737286; PMCID: PMC7395176.

Nagano S, Araki T. 2021. Axonal Transport and Local Translation of mRNA in Neurodegenerative Diseases. Front Mol Neurosci. 14:697973. doi: 10.3389/fnmol.2021.697973. PMID: 34194300; PMCID: PMC8236635.

Nagoshi N, Nakashima H, Fehlings MG. 2015. Riluzole as a neuroprotective drug for spinal cord injury: from bench to bedside. Molecules. 20:7775-7789. doi: 10.3390/molecules20057775. PMID: 25939067; PMCID: PMC6272473.

Nelson AT, Trotti D. 2022. Altered Bioenergetics and Metabolic Homeostasis in Amyotrophic Lateral Sclerosis. Neurotherapeutics. 19:1102-1118. doi: 10.1007/s13311-022-01262-3. PMID: 35773551; PMCID: PMC9587161.

Nishimaru H, Restrepo CE, Ryge J, Yanagawa Y, Kiehn O. 2005. Mammalian motor neurons corelease glutamate and acetylcholine at central synapses. Proc Natl Acad Sci U S A. 102:5245-5249. doi: 10.1073/pnas.0501331102. PMID: 15781854; PMCID: PMC555035.

Nussbacher JK, Tabet R, Yeo GW, Lagier-Tourenne C. 2019. Disruption of RNA Metabolism in Neurological Diseases and Emerging Therapeutic Interventions. Neuron. 102:294-320. doi: 10.1016/j.neuron.2019.03.014. PMID: 30998900; PMCID: PMC6545120.

Pan Q, Shai O, Lee LJ, Frey BJ, Blencowe BJ. 2008. Deep surveying of alternative splicing complexity in the human transcriptome by high-throughput sequencing. Nat Genet. 40:1413-5. doi: 10.1038/ng.259. Erratum in: Nat Genet. 2009. 41:762. PMID: 18978789.

Panda S, Antoch MP, Miller BH, Su AI, Schook AB, Straume M, Schultz PG, Kay SA, Takahashi JS, Hogenesch JB. 2002. Coordinated transcription of key pathways in the mouse by the circadian clock. Cell. 109:307-320. doi: 10.1016/s0092-8674(02)00722-5. PMID: 12015981.

Pantelidou M, Zographos SE, Lederer CW, Kyriakides T, Pfaffl MW, Santama N. 2007. Differential expression of molecular motors in the motor cortex of sporadic ALS. Neurobiol Dis. 26:577-589. doi: 10.1016/j.nbd.2007.02.005. PMID: 17418584.

Patel A, Lee HO, Jawerth L, Maharana S, Jahnel M, Hein MY, Stoynov S, Mahamid J, Saha S, Franzmann TM, et al. 2015. A Liquid-to-Solid Phase Transition of the ALS Protein FUS Accelerated by Disease Mutation. Cell. 162:1066-1077. doi: 10.1016/j.cell.2015.07.047. PMID: 26317470.

Penna MS, Hu RC, Rodney GG, Cooper TA. 2023. The role of *Limch1* alternative splicing in skeletal muscle function. Life Sci Alliance. 6:e202201868. doi: 10.26508/lsa.202201868. PMID: 36977593; PMCID: PMC10052820.

Prashad S, Gopal PP. 2021. RNA-binding proteins in neurological development and disease. RNA Biol. 18:972-987. doi: 10.1080/15476286.2020.1809186. PMID: 32865115; PMCID: PMC8216196.

Preußner M, Goldammer G, Neumann A, Haltenhof T, Rautenstrauch P, Müller-McNicoll M, Heyd F. 2017. Body Temperature Cycles Control Rhythmic Alternative Splicing in Mammals. Mol Cell. 67:433-446. doi: 10.1016/j.molcel.2017.06.006. PMID: 28689656.

Qiu H, Lee S, Shang Y, Wang WY, Au KF, Kamiya S, Barmada SJ, Finkbeiner S, Lui H, Carlton CE, et al. 2014. ALS-associated mutation FUS-R521C causes DNA damage and RNA splicing defects. J Clin Invest. 124:981-999. doi: 10.1172/JCI72723. Erratum in: J Clin Invest. 2021. 131:149564. doi: 10.1172/JCI149564. PMID: 24509083; PMCID: PMC3938263.

Rabin SJ, Kim JM, Baughn M, Libby RT, Kim YJ, Fan Y, Libby RT, La Spada A, Stone B, Ravits J. 2010. Sporadic ALS has compartment-specific aberrant exon splicing and altered cell-matrix adhesion biology. Hum Mol Genet. 19:313-328. doi: 10.1093/hmg/ddp498. PMID: 19864493; PMCID: PMC2796893.

Roenneberg T, Allebrandt KV, Merrow M, Vetter C. 2012. Social jetlag and obesity. Curr Biol. 22:939-943. doi: 10.1016/j.cub.2012.03.038. Erratum in: Curr Biol. 2013. 23:737. PMID: 22578422.

Rossi J, Balthasar N, Olson D, Scott M, Berglund E, Lee CE, Choi MJ, Lauzon D, Lowell BB, Elmquist JK. 2011. Melanocortin-4 receptors expressed by cholinergic neurons regulate energy balance and glucose homeostasis. Cell Metab. 13:195-204. doi: 10.1016/j.cmet.2011.01.010. PMID: 21284986; PMCID: PMC3033043.

Rotundo RL. 2003. Expression and localization of acetylcholinesterase at the neuromuscular junction. J Neurocytol. 32:743-766. doi: 10.1023/B:NEUR.0000020621.58197.d4. PMID: 15034265.

Salton M, Elkon R, Borodina T, Davydov A, Yaspo ML, Halperin E, Shiloh Y. 2011. Matrin 3 binds and stabilizes mRNA. PLoS One. 6:e23882. doi: 10.1371/journal.pone.0023882. PMID: 21858232; PMCID: PMC3157474.

Sanchez SE, Petrillo E, Beckwith EJ, Zhang X, Rugnone ML, Hernando CE, Cuevas JC, Herz MAG, Depetris-Chauvin A, Simpson CG, et al. 2010. A methyl transferase links the circadian clock to the regulation of alternative splicing. Nature. 468:112-116. doi: 10.1038/nature09470. PMID: 20962777.

Sanz E, Yang L, Su T, Morris DR, McKnight GS, Amieux PS. 2009. Cell-type-specific isolation of ribosome-associated mRNA from complex tissues. Proc Natl Acad Sci U S A. 106:13939-13944. doi: 10.1073/pnas.0907143106. PMID: 19666516; PMCID: PMC2728999.

Schmidt HB, Rohatgi R. 2016. In Vivo Formation of Vacuolated Multi-phase Compartments Lacking Membranes. Cell Rep. 16:1228-1236. doi: 10.1016/j.celrep.2016.06.088. PMID: 27452472; PMCID: PMC4972689.

Shannon P, Markiel A, Ozier O, Baliga NS, Wang JT, Ramage D, Amin N, Schwikowski B, Ideker T. 2003. Cytoscape: a software environment for integrated models of biomolecular interaction networks. Genome Res. 13:2498-2504. doi: 10.1101/gr.1239303. PMID: 14597658; PMCID: PMC403769.

Shen S, Park JW, Lu ZX, Lin L, Henry MD, Wu YN, Zhou Q, Xing Y. 2014. rMATS: robust and flexible detection of differential alternative splicing from replicate RNA-Seq data. Proc Natl Acad Sci U S A. 111:E5593-601. doi: 10.1073/pnas.1419161111. PMID: 25480548; PMCID: PMC4280593.

Shinohara K, Funabashi T, Nakamura TJ, Mitsushima D, Kimura F. 2002. Differential regulation of pituitary adenylate cyclase-activating peptide receptor variants in the rat suprachiasmatic nucleus. Neuroscience. 110:301-308. doi: 10.1016/s0306-4522(01)00479-1. PMID: 11958871.

Tada M, Doi H, Koyano S, Kubota S, Fukai R, Hashiguchi S, Hayashi N, Kawamoto Y, Kunii M, Tanaka K, et al. 2018. Matrin 3 Is a Component of Neuronal Cytoplasmic Inclusions of Motor Neurons in Sporadic Amyotrophic Lateral Sclerosis. Am J Pathol. 188:507-514. doi: 10.1016/j.ajpath.2017.10.007. PMID: 29128563.

Tsunematsu T, Yamauchi E, Shibata H, Maki M, Ohta T, Konishi H. 2010. Distinct functions of human MVB12A and MVB12B in the ESCRT-I dependent on their posttranslational modifications. Biochem Biophys Res Commun. 399:232-237. doi: 10.1016/j.bbrc.2010.07.060. Erratum in: Biochem Biophys Res Commun. 2011. 406:158-159. PMID: 20654576.

Ule J, Blencowe BJ. 2019. Alternative Splicing Regulatory Networks: Functions, Mechanisms, and Evolution. Mol Cell. 76:329-345. doi: 10.1016/j.molcel.2019.09.017.

Van Den Bosch L, Van Damme P, Bogaert E, Robberecht W. 2006. The role of excitotoxicity in the pathogenesis of amyotrophic lateral sclerosis. Biochim Biophys Acta. 1762:1068-1082. doi: 10.1016/j.bbadis.2006.05.002. PMID: 16806844.

Vollmers C, Gill S, DiTacchio L, Pulivarthy SR, Le HD, Panda S. 2009. Time of feeding and the intrinsic circadian clock drive rhythms in hepatic gene expression. Proc Natl Acad Sci U S A. 106:21453-21458. doi: 10.1073/pnas.0909591106. PMID: 19940241; PMCID: PMC2795502.

Wang J, Ji X, Liu J, Zhang X. 2019. Serine/Threonine Protein Kinase STK16. Int J Mol Sci. 20:1760. doi: 10.3390/ijms20071760. PMID: 30974739; PMCID: PMC6480182.

Wang KS, Smeyers J, Eggan K, Budnik B, Mordes DA. 2025. C9ORF72 poly-PR disrupts expression of ALS/FTD-implicated *STMN2* through SRSF7. Acta Neuropathol Commun. 13:67. doi: 10.1186/s40478-025-01977-2. PMID: 40140908; PMCID: PMC11948778.

Wang Q, Abruzzi KC, Rosbash M, Rio DC. 2018. Striking circadian neuron diversity and cycling of *Drosophila* alternative splicing. Elife 7:e35618. doi: 10.7554/eLife.35618. PMID: 29863472; PMCID: PMC6025963.

Wijegunawardana D, Nayak A, Vishal SS, Venkatesh N, Gopal PP. 2025. Ataxin-2 polyglutamine expansions aberrantly sequester TDP-43 ribonucleoprotein condensates disrupting mRNA transport and local translation in neurons. Dev Cell. 60:253-269. doi: 10.1016/j.devcel.2024.09.023. PMID: 39419034.

Yang Y, Li Y, Sancar A, Oztas O. 2020. The circadian clock shapes the *Arabidopsi*s transcriptome by regulating alternative splicing and alternative polyadenylation. J Biol Chem. 295:7608-7619. doi: 10.1074/jbc.RA120.013513. PMID: 32303634; PMCID: PMC7261790.

Yeo G, Holste D, Kreiman G, Burge CB. 2004. Variation in alternative splicing across human tissues. Genome Biol. 5:R74. doi: 10.1186/gb-2004-5-10-r74. PMID: 15461793; PMCID: PMC545594.

Young RA, Hagenbüchle O, Schibler U. 1981. A single mouse alpha-amylase gene specifies two different tissue-specific mRNAs. Cell. 23:451-458. doi: 10.1016/0092-8674(81)90140-9. PMID: 6162570.

Zhao M, Kim JR, van Bruggen R, Park J. 2018. RNA-Binding Proteins in Amyotrophic Lateral Sclerosis. Mol Cells. 41:818-829. doi: 10.14348/molcells.2018.0243. PMID: 30157547; PMCID: PMC6182225.

Zhao Q, Hu ZY, Zhang JP, Jiang JD, Ma YY, Li JR, Peng ZG, Chen JH. 2017. Dual Roles of Two Isoforms of Autophagy-related Gene ATG10 in HCV-Subgenomic replicon Mediated Autophagy Flux and Innate Immunity. Sci Rep. 7:11250. doi: 10.1038/s41598-017-11105-3. PMID: 28900156; PMCID: PMC5595887.

Zhou Y, Zhou B, Pache L, Chang M, Khodabakhshi AH, Tanaseichuk O, Benner C, Chanda SK. 2019. Metascape provides a biologist-oriented resource for the analysis of systems-level datasets. Nat Commun. 10:1523. doi: 10.1038/s41467-019-09234-6. PMID: 30944313; PMCID: PMC6447622.

Figure 1

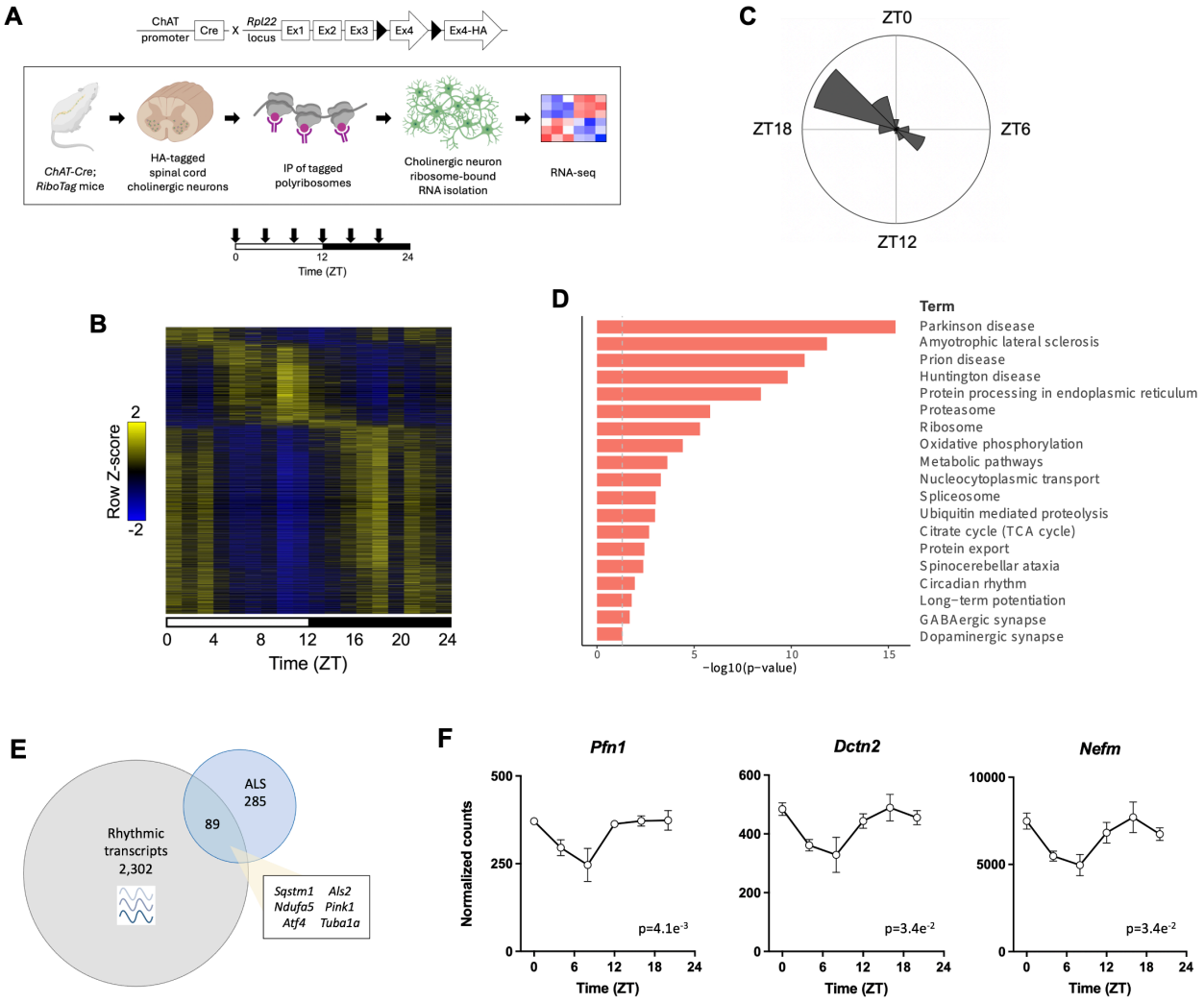
A
ChAT promoter
Cre
X
Rpl22 locus
Ex1
Ex2
Ex3
Ex4
Ex4-HA
ChAT-Cre; RiboTag mice
HA-tagged spinal cord cholinergic neurons
IP of tagged polyribosomes
Cholinergic neuron ribosome-bound RNA isolation
RNA-seq
0
12
24
Time (ZT)
B
Row Z-score
2
-2
0
4
8
12
16
20
24
Time (ZT)
C
ZT0
ZT6
ZT12
ZT18
D
Term
Parkinson disease
Amyotrophic lateral sclerosis
Prion disease
Huntington disease
Protein processing in endoplasmic reticulum
Proteasome
Ribosome
Oxidative phosphorylation
Metabolic pathways
Nucleocytoplasmic transport
Spliceosome
Ubiquitin mediated proteolysis
Citrate cycle (TCA cycle)
Protein export
Spinocerebellar ataxia
Circadian rhythm
Long−term potentiation
GABAergic synapse
Dopaminergic synapse
0
5
10
15
−log10(p−value)
E
ALS
285
89
Rhythmic transcripts
2,302
Sqstm1 Als2
Ndufa5 Pink1
Atf4 Tuba1a
F
Pfn1
Dctn2
Nefm
Normalized counts
500
250
0
600
400
200
10000
5000
p=4.1e-3
p=3.4e-2
p=3.4e-2
0
6
12
18
24
Time (ZT)

Figure 2

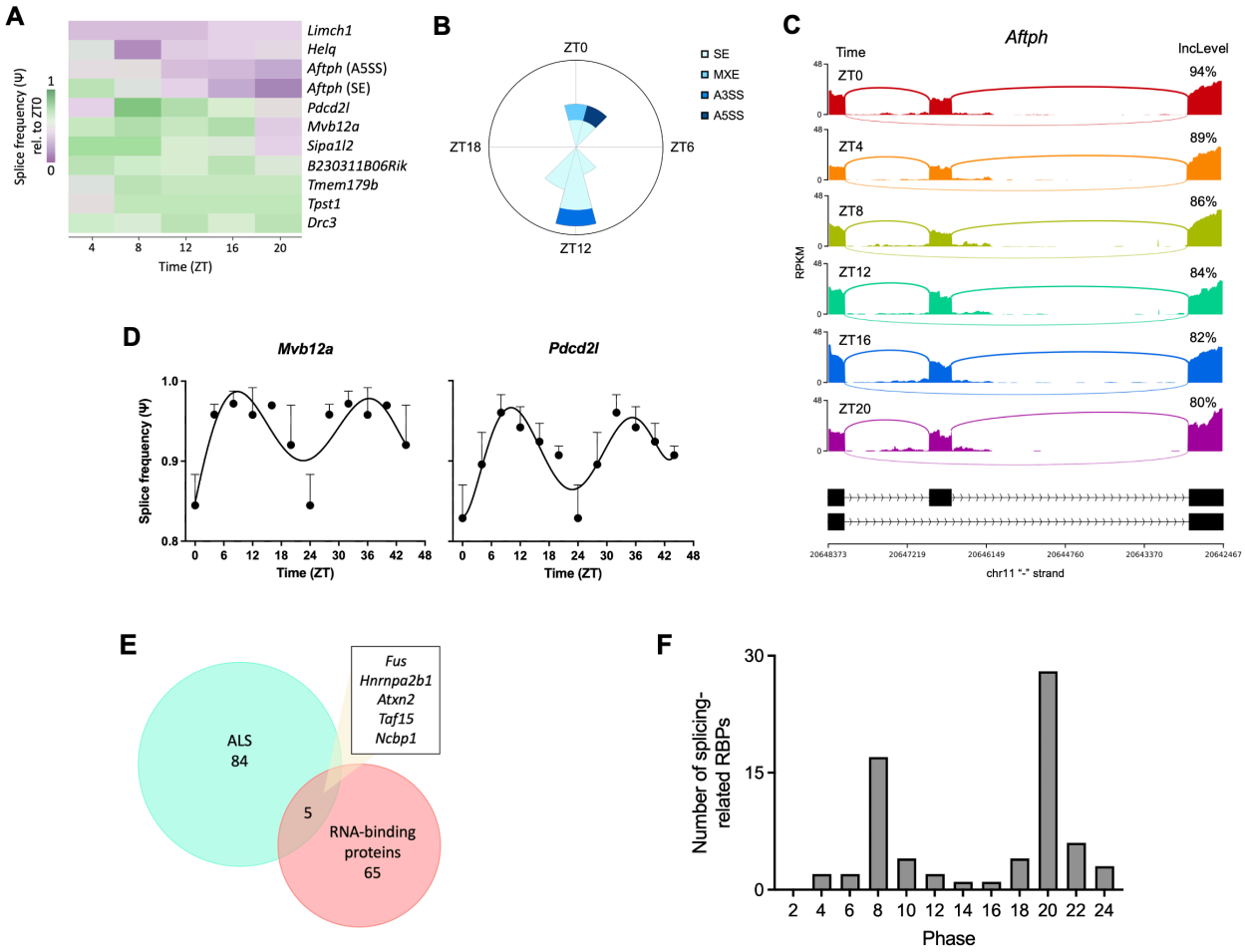
A
Limch1
Helq
Aftph (A5SS)
Aftph (SE)
Pdcd2l
Mvb12a
Sipa1l2
B230311B06Rik
Tmem179b
Tpst1
Drc3
Splice frequency (Ψ) rel. to ZT0
Time (ZT)
B
ZT0
ZT6
ZT12
ZT18
SE
MXE
A3SS
A5SS
C
Aftph
Time
IncLevel
ZT0
94%
ZT4
89%
ZT8
86%
ZT12
84%
ZT16
82%
ZT20
80%
RPKM
chr11 "-" strand
D
Mvb12a
Pdcd2l
Splice frequency (Ψ)
Time (ZT)

E
Fus
Hnrnpa2b1
Atxn2
Taf15
Ncbp1
ALS
84
5
RNA-binding
proteins
65

F
Number of splicing-related RBPs
Phase

Figure 3

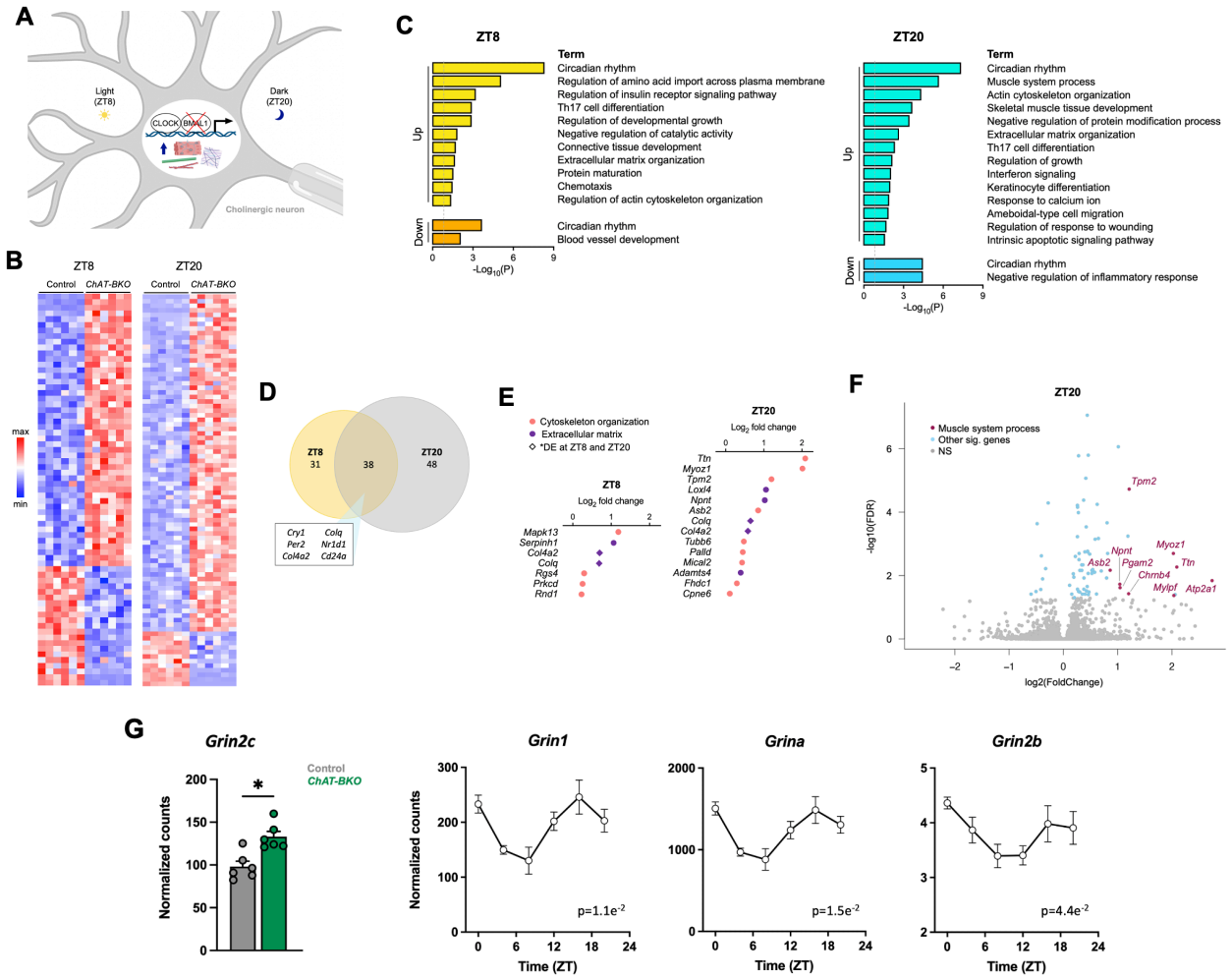
A
Light (ZT8)
Dark (ZT20)
CLOCK
BMAL1
Cholinergic neuron
B
ZT8
ZT20
Control
ChAT-BKO
max
min
C
ZT8
Term
Circadian rhythm
Regulation of amino acid import across plasma membrane
Regulation of insulin receptor signaling pathway
Th17 cell differentiation
Regulation of developmental growth
Negative regulation of catalytic activity
Connective tissue development
Extracellular matrix organization
Protein maturation
Chemotaxis
Regulation of actin cytoskeleton organization
Circadian rhythm
Blood vessel development
Up
Down
-Log10(P)
ZT20
Term
Circadian rhythm
Muscle system process
Actin cytoskeleton organization
Skeletal muscle tissue development
Negative regulation of protein modification process
Extracellular matrix organization
Th17 cell differentiation
Regulation of growth
Interferon signaling
Keratinocyte differentiation
Response to calcium ion
Ameboidal-type cell migration
Regulation of response to wounding
Intrinsic apoptotic signaling pathway
Circadian rhythm
Negative regulation of inflammatory response
D
ZT8 31
38
ZT20 48
Cry1 Colq
Per2 Nr1d1
Col4a2 Cd24a
E
Cytoskeleton organization
Extracellular matrix
*DE at ZT8 and ZT20
ZT8
Log2 fold change
Mapk13
Serpinh1
Col4a2
Colq
Rgs4
Prkcd
Rnd1
ZT20
Log2 fold change
Ttn
Myoz1
Tpm2
Loxl4
Npnt
Asb2
Colq
Col4a2
Tubb6
Palld
Mical2
Adamts4
Fhdc1
Cpne6
F
ZT20
Muscle system process
Other sig. genes
NS
-log10(FDR)
log2(FoldChange)
Tpm2
Myoz1
Npnt
Asb2
Pgam2
Ttn
Chmb4
Mylpf
Atp2a1
G
Grin2c
Control
ChAT-BKO
Normalized counts
Grin1
p=1.1e-2
Grina
p=1.5e-2
Grin2b
p=4.4e-2
Time (ZT)

Figure 4

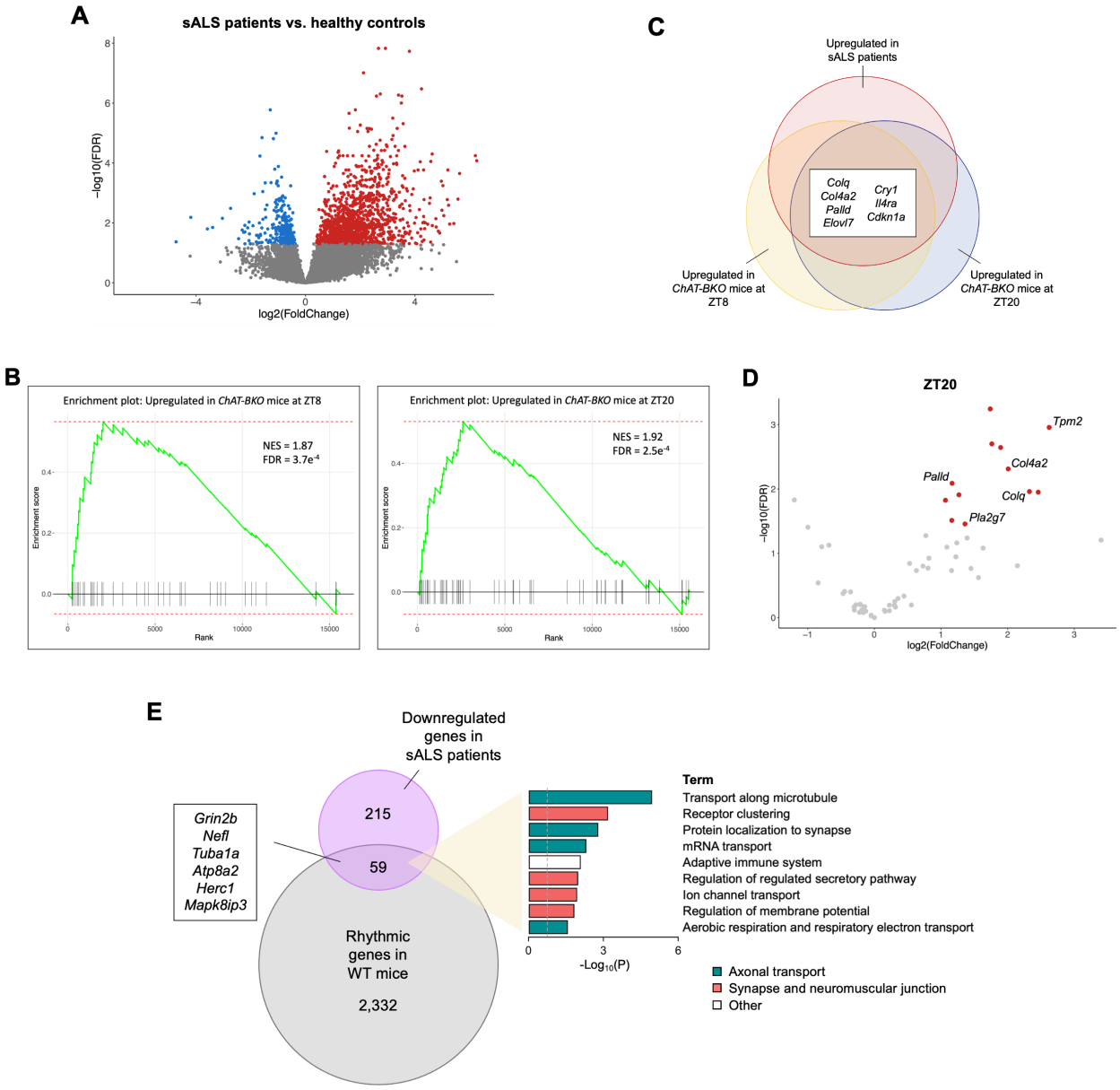
A
sALS patients vs. healthy controls
−log10(FDR)
log2(FoldChange)
C
Upregulated in sALS patients
Colq
Col4a2
Palld
Elovl7
Cry1
Il4ra
Cdkn1a
Upregulated in ChAT-BKO mice at ZT8
Upregulated in ChAT-BKO mice at ZT20
B
Enrichment plot: Upregulated in ChAT-BKO mice at ZT8
NES = 1.87
FDR = 3.7e-4
Enrichment plot: Upregulated in ChAT-BKO mice at ZT20
NES = 1.92
FDR = 2.5e-4
Enrichment score
Rank
D
ZT20
Tpm2
Col4a2
Palld
Colq
Pla2g7
−log10(FDR)
log2(FoldChange)
E
Downregulated genes in sALS patients
215
59
Grin2b
Nefl
Tuba1a
Atp8a2
Herc1
Mapk8ip3
Rhythmic genes in WT mice
2,332
Term
Transport along microtubule
Receptor clustering
Protein localization to synapse
mRNA transport
Adaptive immune system
Regulation of regulated secretory pathway
Ion channel transport
Regulation of membrane potential
Aerobic respiration and respiratory electron transport
-Log10(P)
Axonal transport
Synapse and neuromuscular junction
Other

Figure 5

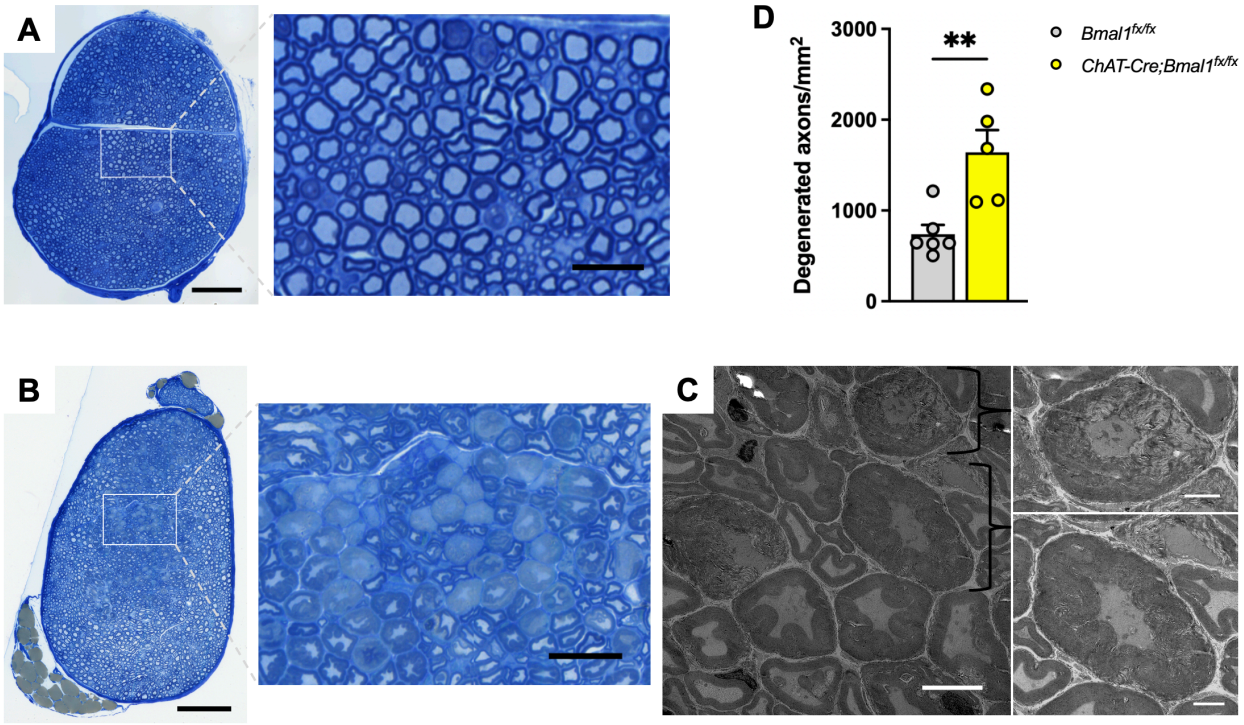
A
B
C
D
Degenerated axons/mm2
3000
2000
1000
0
**
Bmal1fx/fx
ChAT-Cre;Bmal1fx/fx

Figure 6

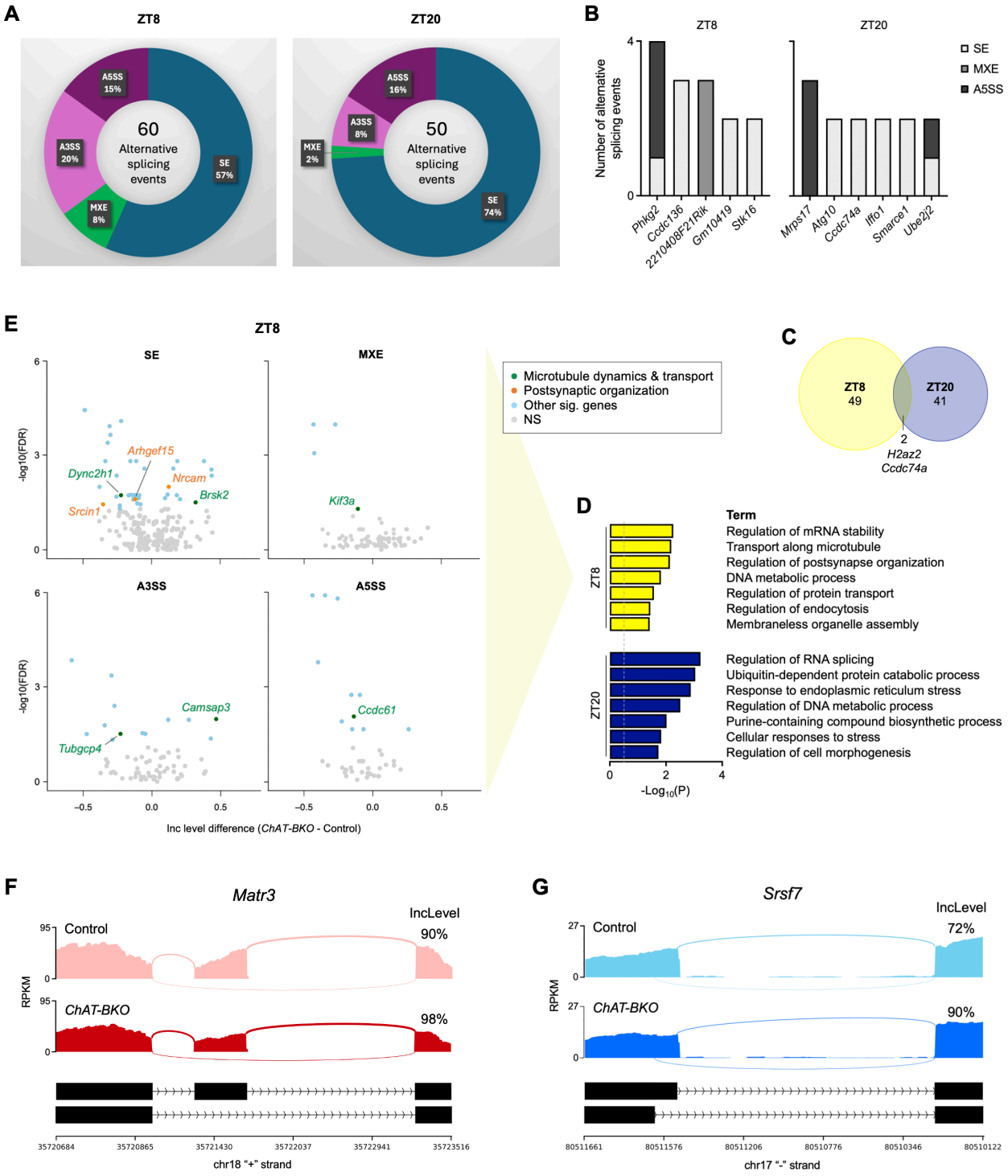
A
ZT8
ZT20
A5SS 15%
A3SS 20%
MXE 8%
SE 57%
60 Alternative splicing events
A5SS 16%
A3SS 8%
MXE 2%
SE 74%
50 Alternative splicing events
B
Number of alternative splicing events
Phkg2
Ccdc136
2210408F21Rik
Gm10419
Stk16
Mrps17
Atg10
Ccdc74a
Iffo1
Smarce1
Ube2j2
SE
MXE
A5SS
C
ZT8 49
ZT20 41
2
H2az2
Ccdc74a
D
Term
Regulation of mRNA stability
Transport along microtubule
Regulation of postsynapse organization
DNA metabolic process
Regulation of protein transport
Regulation of endocytosis
Membraneless organelle assembly
Regulation of RNA splicing
Ubiquitin-dependent protein catabolic process
Response to endoplasmic reticulum stress
Regulation of DNA metabolic process
Purine-containing compound biosynthetic process
Cellular responses to stress
Regulation of cell morphogenesis
-Log10(P)
E
ZT8
SE
MXE
A3SS
A5SS
-log10(FDR)
Arhgef15
Dync2h1
Nrcam
Brsk2
Srcin1
Kif3a
Camsap3
Tubgcp4
Ccdc61
Inc level difference (ChAT-BKO - Control)
Microtubule dynamics & transport
Postsynaptic organization
Other sig. genes
NS
F
Matr3
Control
ChAT-BKO
IncLevel
90%
98%
RPKM
chr18 "+" strand
G
Srsf7
Control
ChAT-BKO
IncLevel
72%
90%
RPKM
chr17 "-" strand

Figure S1

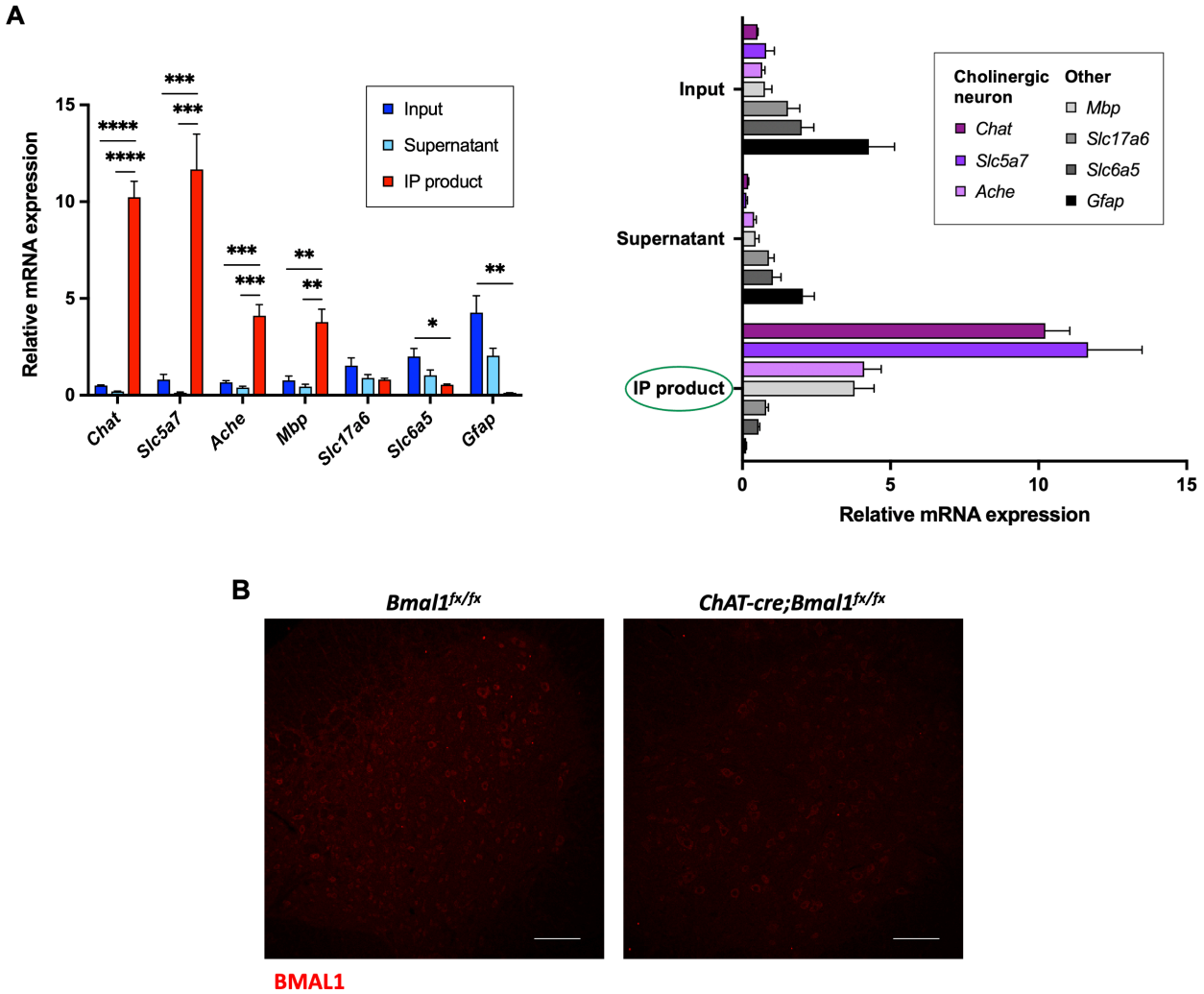

Figure S2

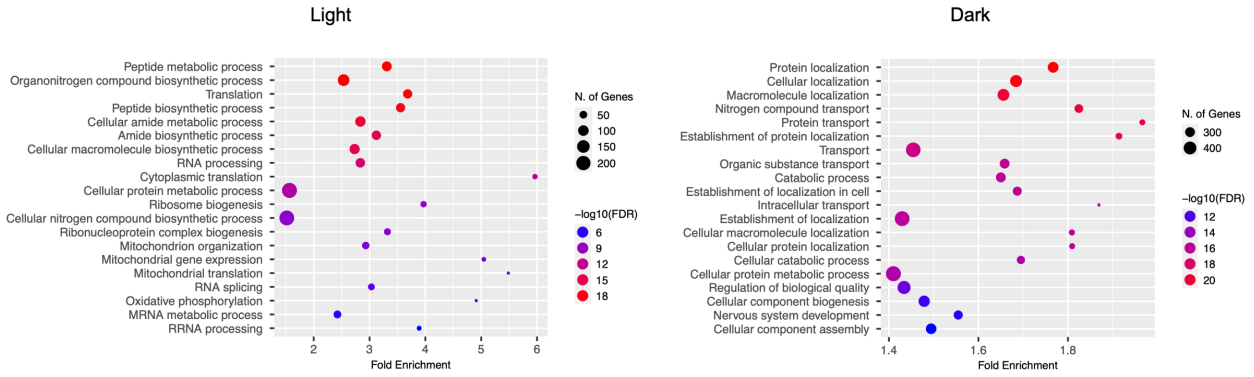

Figure S3

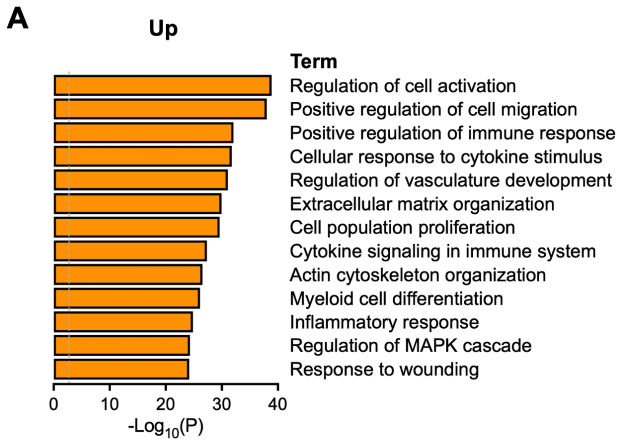
A
Up
Term
Regulation of cell activation
Positive regulation of cell migration
Positive regulation of immune response
Cellular response to cytokine stimulus
Regulation of vasculature development
Extracellular matrix organization
Cell population proliferation
Cytokine signaling in immune system
Actin cytoskeleton organization
Myeloid cell differentiation
Inflammatory response
Regulation of MAPK cascade
Response to wounding
0
10
20
30
40
-Log10(P)

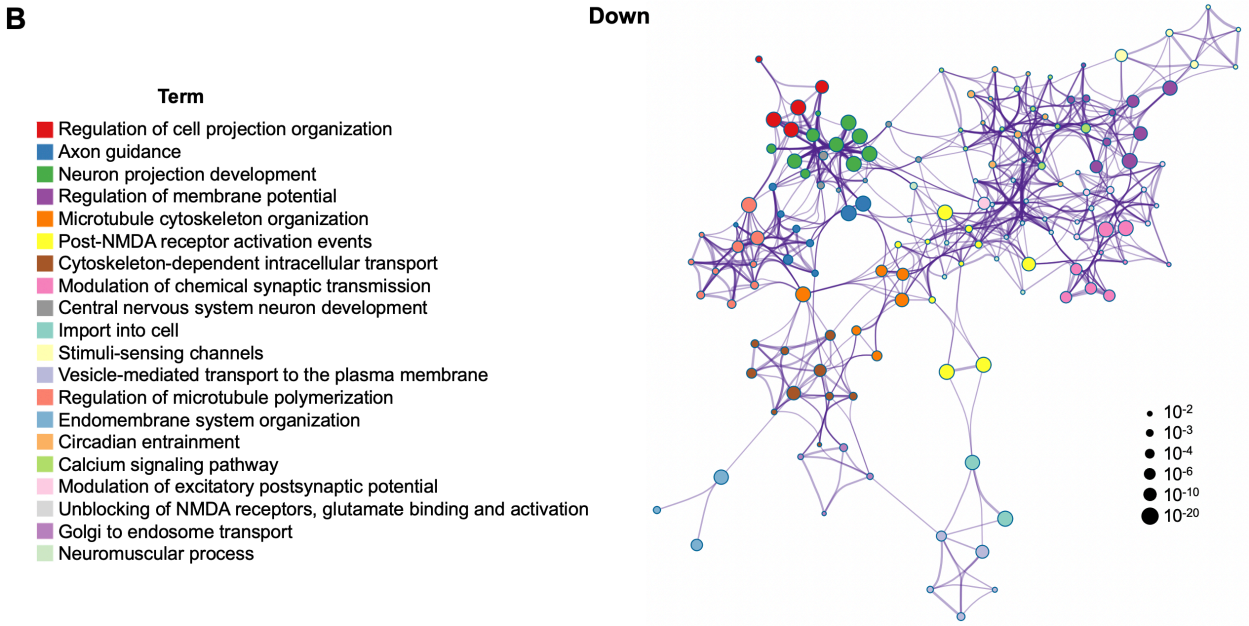
B
Down
Term
Regulation of cell projection organization
Axon guidance
Neuron projection development
Regulation of membrane potential
Microtubule cytoskeleton organization
Post-NMDA receptor activation events
Cytoskeleton-dependent intracellular transport
Modulation of chemical synaptic transmission
Central nervous system neuron development
Import into cell
Stimuli-sensing channels
Vesicle-mediated transport to the plasma membrane
Regulation of microtubule polymerization
Endomembrane system organization
Circadian entrainment
Calcium signaling pathway
Modulation of excitatory postsynaptic potential
Unblocking of NMDA receptors, glutamate binding and activation
Golgi to endosome transport
Neuromuscular process
10-2
10-3
10-4
10-6
10-10
10-20

Figure S4

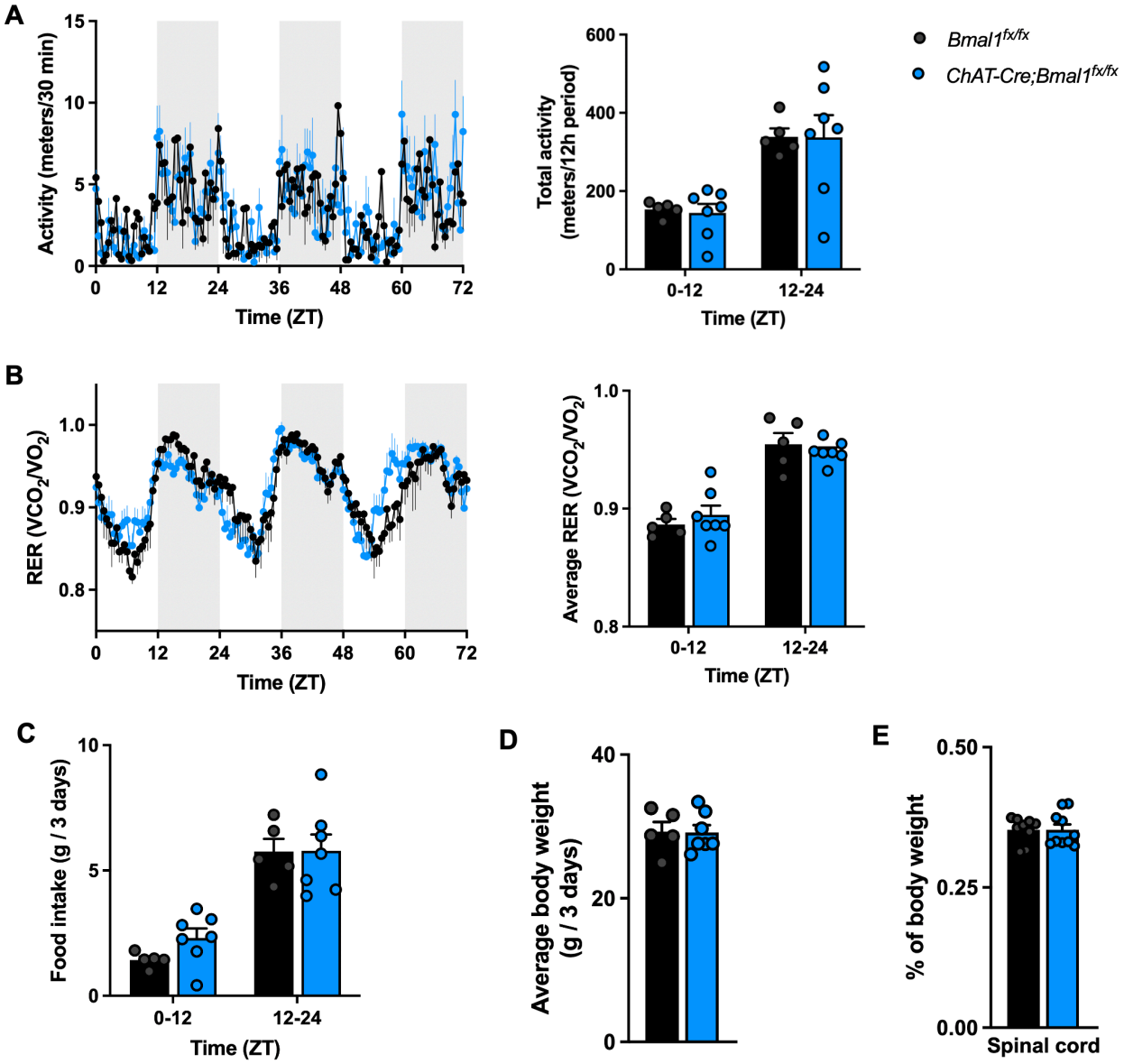
A
Activity (meters/30 min)
Time (ZT)
Total activity (meters/12h period)
0-12
12-24
Time (ZT)
Bmal1fx/fx
ChAT-Cre;Bmal1fx/fx
B
RER (VCO2/VO2)
Time (ZT)
Average RER (VCO2/VO2)
Time (ZT)
C
Food intake (g / 3 days)
Time (ZT)
D
Average body weight (g / 3 days)
E
% of body weight
Spinal cord